國立臺灣大學工學院工程科學及海洋工程學系

碩士論文

Department of Engineering Science and Ocean Engineering

College of Engineering

National Taiwan University

Master’s Thesis

應用於颱風多發的中水深海域之偏軸型半潛之浮式風力發電機繫泊系統之設計與最佳化

Mooring System Design and Optimization for Off-Column Semi-Submersible Floating Wind Turbines in Typhoon-Prone Intermediate Waters

吳冠逸

Kuan-Yi (Zach) Wu

指導教授：馬開東 博士

Advisor: Kai-Tung Ma, Ph.D.

中華民國 114 年 5 月

May 2025

doi:10.6342/NTU202500993

Acknowledgement

My master’s journey at National Taiwan University has been transformative, made possible by the invaluable support and guidance of many individuals and teams.

First, a huge thank you to my supervisor, **Prof. Kai-Tung Ma**. He gave me the chance to pursue this master’s and got me involved in multiple meetings with top offshore wind industry companies, where I even got to present my research. His 30 years experience in the U.S. oil industry taught me how to solve problems smartly and think carefully about my results. He also brought three awesome experts from Houston—**Dr. Yongyan Wu** (Aker Solutions), **Engineer Donghui Chen** (Genesis Engineering LLC), and **Dr. Jer-Fang Wu** (formerly American Bureau of Shipping)—to guide us at NTU. Their knowledge really boosted my work. Special thanks to Dr. Jer-Fang Wu for helping me with research, career tips, and staying positive.

I also want to thank **Prof. Hervé Capart** from the Civil Engineering Department. He got me on the OrthoFloat Team and took us to France for the International Floating Wind Challenge. He drove us to Électricité de France (EDF) and Technip Energies, and we saw the world’s first TLP floating wind farm, Provence Grand Large, plus visited ENSTA Bretagne and Ifremer. These trips showed me how Europe, especially France, builds strong industries with solid ideas. Best of all, I made great friends, **Jojo Chih-Hua Jen** and **Diego Alejandro Hernandez Machado**, and we learned “stand by” from 卡哥!

Outside school, thanks to **Regruto Jean-Loup Axel** and **Maya Davita Athalia** for always being there and keeping me active. You helped me stay healthy and happy.

Big thanks to **Dr. Amir Noorizadegan** for his insightful guidance. His support greatly strengthened both my thesis and papers.

Finally, thanks to **Prof. Lin Tsung-Yueh**, **Prof. Chau Shiu-Wu**, and their teams for the data, and to all members in the **Offshore Structure and Mooring Engineering Lab** and **TaidaFloat research teams** (CSBC Corporation Taiwan, Ship and Ocean Industries R&D Center (SOIC)) for making this thesis possible.

doi:10.6342/NTU202500993

摘要

本論文針對目前學術界對於偏軸型半潛（off-column semisubmersible）之浮式風機在颱風與中水深結合條件下繫泊研究的不足，研究了一種 15 兆瓦偏軸式半潛式浮式離岸風力發電機臺大浮臺（TaidaFloat），在臺灣海峽 70 公尺的中水深且多颱風的環境下，懸鏈式繫泊系統（catenary mooring system）的設計與優化。本研究使用 ANSYS SpaceClaim、ANSYS Aqwa、OrcaWave 和 OrcaFlex 開發了全面數值框架，模擬浮台水動力學與繫泊動態。此研究中的水動力參數已通過實驗數據驗證，並納入計算流體力學（CFD）計算的阻力係數以考慮風與洋流負載。 本論文使用 Python，基於最可能最大值（MPM）方法估算極端繫泊張力，避免過度保守的設計結果。3x3 全鏈繫泊系統經優化，實現 1,190 公尺錨固半徑，並進一步通過每條繫泊線整合 12 個 8 噸重的配重塊，減少 29% 錨固半徑至 840 公尺，提升繫泊剛性並降低浮台位移和最大繫泊線張力。研究顯示偏軸設計引發偏航（sway）旋轉，增加繫泊張力，使繫泊系統設計面臨挑戰。這些發現為多颱風的中水深環境下，偏軸式半潛式風機的繫泊設計提供關鍵見解。

關鍵詞：浮式風力發電機、偏軸式半潛式浮臺、颱風、中水深、繫泊系統、加重塊

doi:10.6342/NTU202500993

Abstract

This thesis addresses the gap in mooring studies for off-column semi-submersibles in typhoon-prone intermediate-depth conditions by investigating the design and optimization of a catenary mooring system for TaidaFloat, a 15 MW off-column semi-submersible floating offshore wind turbine (FOWT) deployed in the 70 m deep waters of the Taiwan Strait. A robust numerical framework, integrating ANSYS SpaceClaim, ANSYS Aqwa, OrcaWave, and OrcaFlex, is developed to model platform hydrodynamics and mooring dynamics. The hydrodynamic properties are validated against experimental data, incorporating computational fluid dynamics-derived drag coefficients to account for wind and current loads. Utilizing Python, the study applies the Most Probable Maximum (MPM) method to estimate extreme mooring tensions, ensuring practical designs that avoid overly conservative outcomes. The optimized 3x3 all-chain mooring system achieves a 1,190 m anchor radius, reduced by 29% to 840 m through the addition of 12 8-tonne clump weights per line, enhancing stiffness and minimizing offset and tension. The analysis reveals that off-column designs induce yaw rotation, leading to increased mooring tension and posing challenges to mooring system design. These findings provide essential insights for the mooring design of off-column semi-submersible wind turbines in typhoon-prone intermediate-depth environments.

Keywords：Floating Offshore Wind Turbine, off-column semi-submersible, Typhoon, Intermediate Water, Mooring System, Clump Weight

doi:10.6342/NTU202500993

Contents

doi:10.6342/NTU202500993

doi:10.6342/NTU202500993

doi:10.6342/NTU202500993

List of Tables

doi:10.6342/NTU202500993

doi:10.6342/NTU202500993

List of Figures

doi:10.6342/NTU202500993

doi:10.6342/NTU202500993

1 Introduction

1.1 Background and Motivation

The Paris Agreement [1] set an ambitious target to limit global warming to 1.5°C above pre-industrial levels by 2100, necessitating net-zero CO_2 emissions worldwide by 2050. To achieve this, the International Energy Agency's (IEA) Net Zero Roadmap [2] outlines a pathway to eliminate CO_2 emissions from the global energy sector by 2050, with wind power playing a pivotal role. The roadmap projects a global wind capacity of 2.75 TW by 2050, underscoring the importance of both onshore and offshore wind technologies.

Since the installation of the first bottom-fixed offshore wind turbine in 1990 [3, 4], offshore wind technology has advanced significantly. Initially limited to shallow coastal waters, the industry has progressively expanded into deeper waters to capture stronger, more consistent winds for greater energy yield. In this thesis, "shallow water" is defined as depths less than 50 meters, "intermediate water" refers to depths ranging from approximately 50 to 80 meters, and "deep water" corresponds to depths exceeding 100 meters. Figure 1 illustrates the progression of fixed-bottom offshore wind farms, showing the average water depth over time. It took approximately 16 years to reach an average depth of 20 meters, followed by a rapid advance to 30 meters in three years. Progress then

doi:10.6342/NTU202500993

slowed, requiring about 10 years to reach 40 meters and longer to achieve 50 meters. This deceleration highlights the technical and economic challenges of deploying bottom-fixed structures beyond shallow waters, driving the development of floating offshore wind turbines (FOWTs) for intermediate and deep waters.

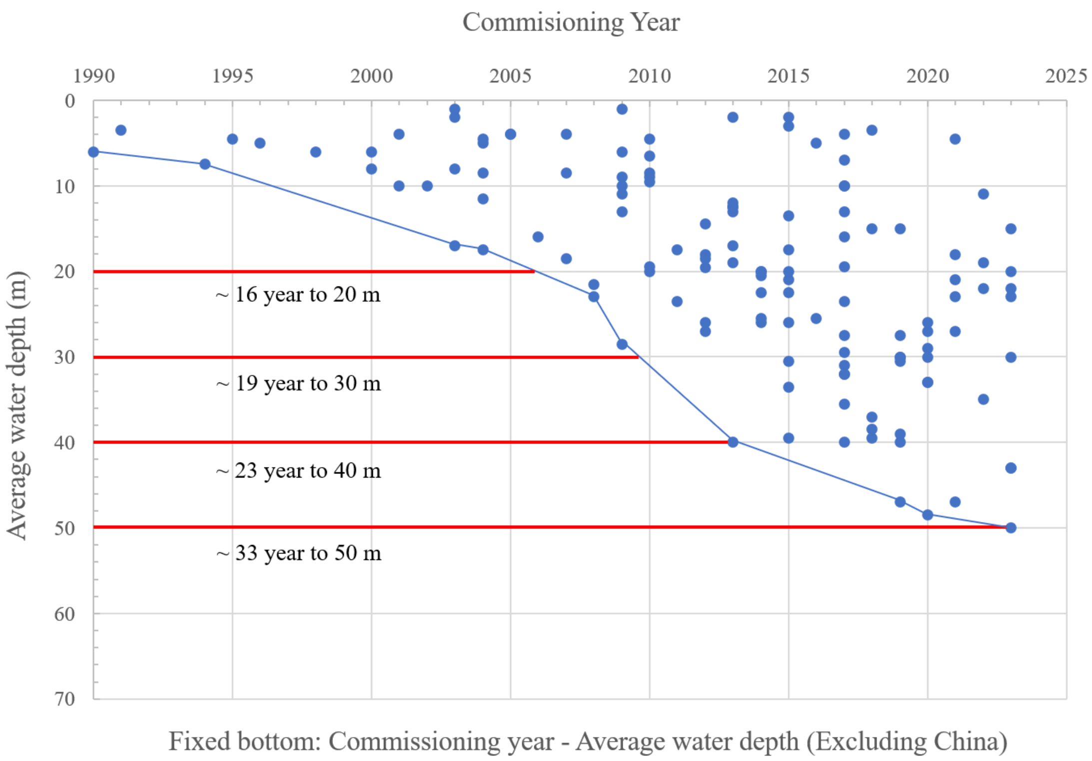

Figure 1: Evolution of Average Water Depth in Fixed-Bottom Offshore Wind Farms Over Time

This study focuses on the Taiwan Strait, an emerging hub for offshore wind in Asia. Several bottom-fixed offshore wind farms operate in shallow waters, but these sites are nearing full utilization. With limited deep-water sites exceeding 100 meters in the region, developers are targeting intermediate water depths of 60 to 70 meters off Hsinchu's coast for floating wind farms.

doi:10.6342/NTU202500993

Globally, FOWTs have progressed, with several operational projects. Table 1 categorizes these by floater type, detailing project numbers and capacities. To assess technology readiness levels (TRL), projects are classified as demonstration (single-unit) or scaled (multi-unit). Semi-submersibles and spar-type platforms lead, with higher TRLs than barges and tension-leg platforms (TLPs). Semi-submersibles dominate with 11 projects, including three scaled projects (WindFloat Atlantic, Kincardine, and Golfe du Lion) and eight demonstrations (WindFloat 1, Eolink Demo, Fukushima Mirai, Fukushima Shimpuu, Yangxi Shanpa III Demo, Fuyao Prototype, Haiyou Guanlan, and OceanX). Spar-type platforms follow with six projects, including two scaled (Hywind Scotland and Hywind Tampen) and four demonstrations (Hywind Demo, Haenkaze, Fukushima Hamakaze, and TetraSpar Demo).

Table 1: Numbers of Operated Projects by Floater Types

Type	Scale	No. of the projects	Project Name	Project Capacity (MW)	Total capacity of all projects
Barge	Demo	3	Floatgen	2	7 MW
			Hibiki	3	
			DemoSATH	2	
Spar buoy	Scaled (>1 unit)	2	Hywind Scotland	30	130.9 MW
			Hywind Tampen	88	
	Demo	4	Hywind Demo	2.3	
			Haenkaze/Sakiyama	2	
			Fukushima Hamakaze	5	
			TetraSpar Demo	3.6	
TLP	Scaled (>1 unit)	1	Provence Grand Large	25	25.225 MW
	Demo	1	PivotBuoy	0.225	
Semi-sub	Scaled (>1 unit)	3	WindFloat Atlantic	25	156.55 MW
			Kincardine	50	
			Golfe du Lion	30	
	Demo	8	WindFloat 1	2	
			Eolink Demo (France Atlantic)	5	
			Fukushima Mirai	2	
			Fukushima Shimpuu	7	
			Yangxi Shapa III demo	5.5	
			FuYao prototype	6.2	
			Haiyou Guanlan	7.25	
			OceanX	16.6	

doi:10.6342/NTU202500993

However, conventional spar-type platforms, such as those by Nielsen et al. [5], require deep drafts, making them only suitable for deep waters exceeding 100 meters [6]. Although innovative spar designs aim to overcome these limitations (see Figure 2), they lack real-sea validation and are not viable for intermediate waters. Semi-submersibles, with their high TRL and adaptability to intermediate depths, are thus the focus of this thesis.

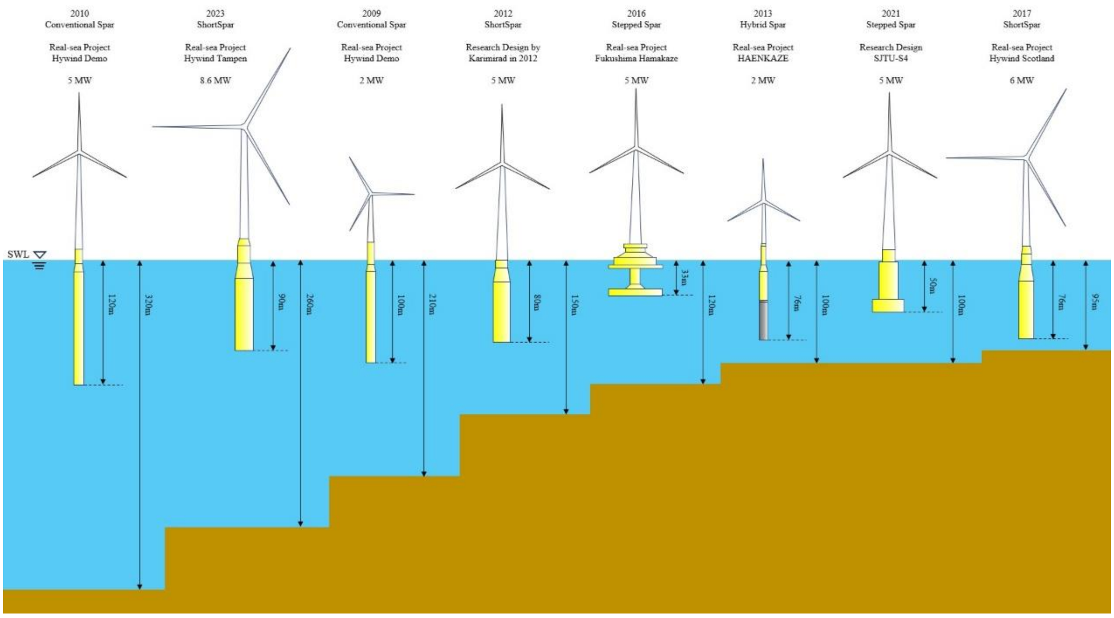

Figure 2: The Draft and Water Depth of Different Spar Designs

1.2 Types of Mooring System

Mooring systems for FOWTs are broadly classified into catenary and taut systems, as depicted in Figure 3. In a catenary mooring system, part of the mooring line rests on the seabed in static equilibrium, forming a catenary shape due to its weight. This configuration provides flexibility to accommodate the floater’s dynamic movements and

doi:10.6342/NTU202500993

positional shifts, making it well-suited for intermediate water depths. In contrast, a taut mooring system features fully suspended lines between the seabed anchor and the floater, resulting in a smaller seabed footprint and reduced material requirements. However, taut systems rely on elastic stretching for compliance, leading to increased stiffness and tension in intermediate waters, rendering them more appropriate for deep or ultra-deep environments.

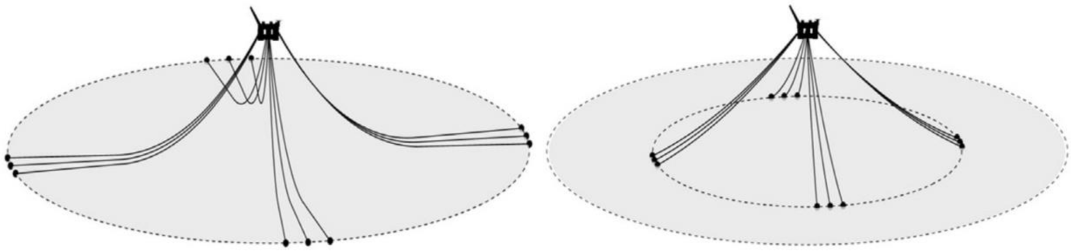

Figure 3: (Left) Catenary mooring system. (Right) Taut mooring system. [7]

In intermediate water depths, catenary moorings excel because their suspended lines provide sufficient restoring forces through weight and curvature, effectively managing surge and sway motions critical for semi-submersibles [8]. Unlike taut moorings, which require deeper waters for compliance, catenary systems adapt well to this depth range. Additionally, their design allows a portion of the line to rest on the seabed, reducing vertical loads on anchors and simplifying anchor requirements compared to taut systems [9]. Given these advantages, this study focuses on catenary mooring systems in intermediate water depths.

doi:10.6342/NTU202500993

1.3 Literature Review on Catenary Mooring System in Intermediate water and Typhoon Environment

Mooring systems in intermediate waters (50-80m), as defined in this thesis, exhibit distinct structural characteristics compared to deep-water (>100 meters) systems, necessitating specialized design approaches. In intermediate waters, nonlinear wave excitation is more pronounced, and semi-submersible platforms are particularly susceptible to significant offsets driven by slow-drift forces. These challenges have been extensively studied in fields such as offshore oil and gas and FOWTs. This section provides a concise overview of relevant research.

Brommundt et al. [10] employed frequency-domain analysis to study catenary mooring systems for a center-column FOWT at water depths of 75 meters and 330 meters, highlighting the importance of considering spectral wind loads in mooring design. Benassai et al. [11] compared catenary chain mooring systems for a 5 MW center-column FOWT at depths ranging from 50 to 200 meters, finding that in intermediate waters, heavier mooring chains are required to limit platform offset, indicating reduced performance. Similarly, Campanile et al. [12] analyzed catenary chain mooring systems for a 5 MW center-column FOWT at depths of 50 to 80 meters, noting that the total weight of mooring chains increases significantly as water depth decreases, underscoring the

doi:10.6342/NTU202500993

challenges of catenary systems in intermediate waters.

Adding clump weights is a recognized approach to enhance catenary mooring performance. Hordvik [13] investigated the impact of clump weight mass on mooring line conformation for a spar-type FOWT, finding that larger clump weights better constrain platform offset within the mooring line's maximum tension limits. Pan et al. [14] analyzed the effect of a 40-ton clump weight on a center-column semi-submersible FOWT, reporting a 14% reduction in mooring line length, a 15% smaller mooring footprint, and a 9% decrease in maximum tension, though maximum surge increased by 25%. Most clump weight studies focus on deep waters exceeding 100 meters, with limited research on for intermediate depths of 50 to 80 meters. Xu [15] analyzed mooring line behavior for a center-column semi-submersible FOWT across various depths, recommending catenary mooring systems with clump weights for intermediate waters at 50 meters.

With the rise of floating wind development in Asia, the impact of typhoons on FOWTs has gained significant attention. Li et al. [16] assessed a 50-ton clump weight on a 10 MW center-column semi-submersible FOWT in 130-meter deep water under typhoon conditions, demonstrating that clump weights effectively reduce surge motion and tension fluctuations.

doi:10.6342/NTU202500993

1.4 Challenges & Objectives

This study focuses on a potential floating wind farm site off Hsinchu's coast in the Taiwan Strait, characterized by intermediate water depths of 70 meters and frequent typhoons. Designing mooring systems for FOWTs in this environment is challenging due to the combined effects of intermediate depths and extreme typhoon conditions. The literature indicates that clump weights enhance mooring performance in both typhoon-prone and intermediate-depth environments. However, several gaps remain, which this thesis aims to address:

1. **Focus on Center-Column Designs**: Mooring studies for semi-submersibles exclusively target center-column designs, such as the open-source OC4 semi-submersible [17] and UMaine VolturnUS semi-submersible [18] as shown in Figure 4, due to their prevalence in research. In contrast, the only two commercially operational semi-submersible wind farms, WindFloat Atlantic and Kincardine, utilize off-column semi-submersible designs, validated in real-sea conditions and likely a leading choice for Taiwan's future floating wind farms. The distinct structural configurations of off-column and center-column semi-submersibles lead to different hydrodynamic properties and motion responses. The mooring system performance of off-column semi-submersibles in the typhoon-prone, intermediate-

doi:10.6342/NTU202500993

depth waters of the Taiwan Strait remains underexplored.

Figure 4: Center-column Platform (Left; VolturnUS [18]) and Off-column Platform (Right; WindFloat Atlantic [19], Courtesy of *Principle Power*)

2. **Limited Research on Combined Typhoon and Intermediate-Depth Conditions:** Existing research typically examines clump weights under either typhoon conditions or intermediate depths in isolation. There is a notable lack of studies addressing the combined effect of clump weights in environments with both frequent typhoons and intermediate water depth.

3. **Unrealistic Clump Weight Masses**: Most studies consider large clump weights, often exceeding 30 tons, which differ significantly from practical offshore engineering practices that typically use multiple clump weights of up to 10 tons each. This discrepancy leads to substantial errors in estimating mooring tension and platform motion.

doi:10.6342/NTU202500993

4. **Omission of Environmental Loads**: Due to the absence of directional drag coefficient data in reports for open-source designs like OC4 semi-submersible and UMaine VolturnUS, most studies neglect current and wind loads acting on the floater. This omission significantly underestimates extreme environmental forces during typhoons.

To address these challenges, the main objectives of this thesis are:

1. **Design and Model an Off-Column Semi-Submersible**: Develop TaidaFloat, an off-column semi-submersible carrying an IEA 15 MW turbine [20], based on ABS stability requirements [21]. Conduct numerical diffraction analysis to obtain the floater's first-order wave excitation, validated with experimental data. Given that nonlinear wave excitation is pronounced in intermediate waters, where semi-submersibles are susceptible to slow-drift-induced offsets, compute second-order wave excitation using full quadratic transfer functions (QTF). To account for current and wind loads, incorporate drag coefficients derived from computational fluid dynamics (CFD) into the model. This comprehensive hydrodynamic model will elucidate the distinct mooring system design considerations for off-column semi-submersibles compared to center-column designs.

2. **Simulate Typhoon and Intermediate-Depth Conditions**: Use the water depth

doi:10.6342/NTU202500993

offshore Hsinchu (70 meters) and 50-year return period wind, wave, and current data as environmental conditions in a fully coupled time-domain simulation. Based on these conditions, design a catenary chain mooring system for the FOWT, addressing the combined challenges of typhoons and intermediate water depths.

3. **Realistic Mooring Design with Clump Weights**: Drawing on the thesis advisor's extensive offshore engineering experience, adopt a maximum chain size of 170 mm and multiple 8-ton clump weights, aligning with practical engineering practices. This approach will enable a realistic mooring design, allowing an assessment of the impact of practical clump weight configurations on mooring performance in the typhoon-prone, intermediate-depth environment of the Taiwan Strait.

The semi-submersible is selected as the target floater type due to its proven applicability in intermediate waters, as discussed earlier. This thesis consolidates the work conducted over the author's two-year master's program, drawing upon a conference paper, an industrial report, a technical specification, and an unpublished journal manuscript, all included in Appendix A.

1.5 Thesis Outline

This thesis investigates the design and optimization of a mooring system for the TaidaFloat, an off-column semi-submersible FOWT, in the typhoon-prone intermediate

doi:10.6342/NTU202500993

waters of the Taiwan Strait. It is organized into nine chapters, covering background, methodology, design, validation, and optimization. Below is a concise outline of the thesis structure:

- **Chapter 1: Introduction and Background**

Introduces offshore wind energy, focusing on FOWTs in the Taiwan Strait (70 m depth). Defines water depths, reviews catenary and taut mooring systems, and identifies research gaps in off-column semi-submersible designs under typhoon conditions. Outlines objectives: design TaidaFloat, simulate typhoon conditions, and develop a realistic mooring system.

- **Chapter 2: Research Methodology**

Describes the numerical framework using ANSYS SpaceClaim, ANSYS Aqwa, OrcaWave, OrcaFlex, and the MPM method for modeling and analyzing FOWT dynamics, ensuring accurate hydrodynamic and mooring system simulations.

- **Chapter 3: Design Basis**

Specifies environmental conditions (50-year return period: 57 m/s wind, 12.72 m wave, 1.59 m/s current) and mooring chain (170 mm R4S-grade, 10 mm corrosion allowance) for the Hsinchu site, based on ABS rules for DLC 6.1.

doi:10.6342/NTU202500993

- **Chapter 4: TaidaFloat Platform Description**

Details the TaidaFloat's hexagonal flat-plate semi-submersible design for a 15 MW turbine, highlighting its stability, manufacturability, and properties (21,028 t displacement, 20 m draft).

- **Chapter 5: Numerical Model Validation of TaidaFloat**

Validates the TaidaFloat numerical model using OrcaWave for hydrodynamic analysis (first- and second-order wave forces) and CFD-derived drag coefficients, comparing results with experimental data.

- **Chapter 6: Design Requirements**

Outlines mooring system requirements per ABS standards: maximum tension (safety factor 1.67, 24,281 kN MBL), maximum offset (21 m).

- **Chapter 7: Design and Optimization of All-Chain Mooring System**

Designs a 3x3 all-chain catenary mooring system with 6.6% MBL pre-tension at a 1,190 m anchor radius, meeting tension and offset standards for typhoon conditions.

- **Chapter 8: Clump-Weighted All-Chain Mooring**

Design and Optimization 1 Enhances the mooring system with 8-ton clump weights (12 per line, 100 m from fairlead) at an 840 m anchor radius, reducing the footprint by

doi:10.6342/NTU202500993

29% while complying with design standards.

- **Chapter 9: Conclusions**

Summarizes findings on off-column design challenges, clump weight effectiveness, current load impacts, and MPM method efficiency. Recommends center-column designs and future research for optimized FOWTs.

- **Appendices**

Includes conference papers, reports, specifications, and the MPM Python script, consolidating two years of research outputs.

This structure provides a clear progression from context to practical mooring system solutions for the Taiwan Strait’s challenging environment.

doi:10.6342/NTU202500993

2 Research Methodology

2.1 Numerical Framework

The numerical framework developed in this study integrates a suite of computational tools to model and analyze the dynamic behavior of a FOWT. This framework combines computer-aided design (CAD), hydrodynamic analysis, and time-domain dynamic simulations to ensure a comprehensive assessment of the platform's stability, hydrodynamic performance, and mooring system response. The methodology leverages industry-standard software tools—ANSYS SpaceClaim, ANSYS Aqwa, OrcaWave, and OrcaFlex—to construct a robust pipeline from geometric modeling to dynamic response prediction. Each tool addresses a specific aspect of the analysis, with data seamlessly transferred between them to maintain consistency and accuracy. Figure 5 illustrates the workflow of this numerical framework, highlighting the sequential integration of modeling, meshing, hydrodynamic analysis, dynamic simulation, and statistical post-processing.

doi:10.6342/NTU202500993

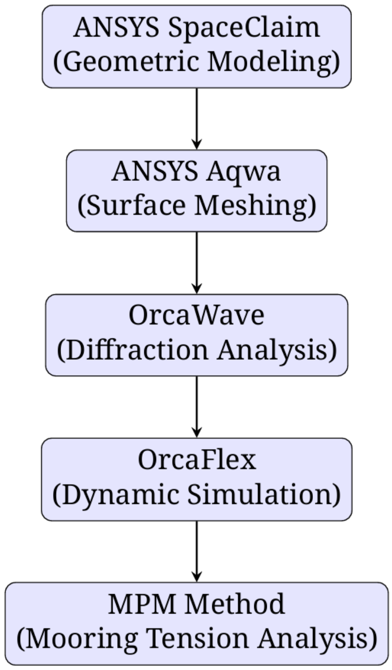

Figure 5: Workflow of the numerical framework for FOWT analysis, integrating ANSYS SpaceClaim, ANSYS Aqwa, OrcaWave, OrcaFlex, and the MPM method

The process begins with the creation of a detailed three-dimensional (3D) geometric model of the FOWT platform in ANSYS SpaceClaim, as described in Section 2.2. This parametric CAD model captures the hull geometry, including critical structural components such as pontoons, columns, and the tower base, ensuring an accurate representation of the platform's wetted surface and mass distribution. The model is then imported into ANSYS Aqwa for surface meshing, as outlined in Section 2.3, where a high-quality mesh is generated to support hydrodynamic calculations. The meshed geometry is subsequently analyzed in OrcaWave (Section 2.4) to perform frequency-domain diffraction analysis, computing hydrodynamic coefficients and wave-induced forces using potential flow theory and boundary element methods (BEM). These results

doi:10.6342/NTU202500993

are transferred to OrcaFlex for time-domain dynamic simulations (Section 2.5), which model the platform's motion and mooring system response under combined wave, wind, and current loads. Finally, a statistical approach, the Most Probable Maximum (MPM) method, is employed to estimate extreme mooring tensions, as detailed in Section 2.6, using a Python-based post-processing script to analyze simulation outputs.

2.2 Platform Model Development in ANSYS SpaceClaim

The initial step involves constructing a detailed three-dimensional (3D) geometric model of the FOWT platform using ANSYS SpaceClaim. This software facilitates the creation of a parametric CAD model, representing the hull geometry of the floating platform. The model includes critical structural components such as the pontoons, columns, and tower base, ensuring accurate representation of the platform's external wetted surface and mass distribution. The geometry is defined to align with design specifications, such as draft, displacement, and overall dimensions, which are essential for subsequent hydrodynamic and stability analyses.

2.3 Meshing in ANSYS Aqwa

The geometric model is imported into ANSYS Aqwa for meshing, which is a prerequisite for hydrodynamic analysis. Aqwa generates a surface mesh of the wetted hull using triangular or quadrilateral elements, ensuring sufficient resolution to capture wave-

doi:10.6342/NTU202500993

structure interactions. The mesh quality—characterized by element size, aspect ratio, and skewness—directly affects the accuracy of subsequent diffraction and radiation calculations. In this study, the maximum mesh size was set to 2 meters. A finer mesh is applied near complex geometric features (e.g., sharp edges or small-diameter columns) to resolve local flow effects, while coarser elements are sufficient for flat surfaces. The meshed model is exported in a format (.dat) compatible with OrcaWave, retaining the hydrodynamic panel representation. Figure 6 shows the completed mesh file imported into OrcaWave.

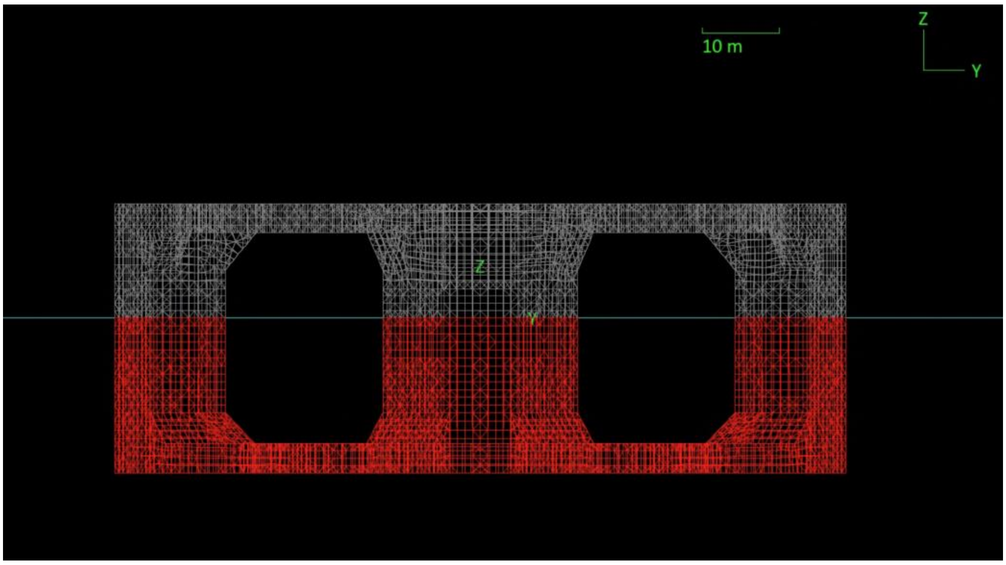

Figure 6: Surface Mesh of TaidaFloat Imported into OrcaWave

2.4 Diffraction Analysis in OrcaWave

OrcaWave is employed to perform a frequency-domain diffraction analysis, calculating the hydrodynamic loads and motion responses of the floating platform under incident wave conditions. This analysis leverages potential flow theory and boundary

doi:10.6342/NTU202500993

element methods (BEM) to model wave-structure interactions, providing the hydrodynamic coefficients and forces imported into OrcaFlex.

2.4.1 Governing Equations

OrcaWave assumes the fluid is incompressible, inviscid, and irrotational, enabling the velocity field to be expressed as the gradient of a scalar potential $\phi(\vec{r}, t)$, where $\vec{r} = (x, y, z)$. This potential satisfies Laplace's equation throughout the fluid domain:

$$\nabla^2 \phi = 0 \tag{1}$$

For harmonic wave motion, the potential is time-dependent and separable as $\phi(\vec{r}, t) = Re[\Phi(\vec{r})e^{-i\omega t}]$, where $\Phi(\vec{r})$ is the complex spatial potential and ω is the wave frequency. The total potential is decomposed into incident, diffraction, and radiation components:

$$\Phi = \Phi_I + \Phi_D + \sum_{j=1}^{6} \Phi_{R,J} \dot{x}_j, \tag{2}$$

where:

- Φ_I is the incident wave potential, representing undisturbed incoming waves.
- Φ_D is the diffraction potential, resulting from wave scattering by the fixed platform.
- $\Phi_{R,J}$ is the radiation potential for the j-th degree of freedom (surge, sway, heave, roll, pitch, yaw), proportional to the platform's velocity $\dot{x}_J$

doi:10.6342/NTU202500993

2.4.2 Hydrodynamic Forces

Hydrodynamic forces and coefficients are computed by integrating pressures over the platform's wetted surface, derived from the linearized Bernoulli equation:

$$p = -\rho \frac{\partial \phi}{\partial t} = i\omega\rho\Phi e^{-i\omega t}, \tag{3}$$

where ρ is the water density. These forces include first-order and second-order contributions, reflecting OrcaWave's full quadratic transfer function (QTF) capability.

First-Order Forces

The first-order wave excitation force in the i-th degree of freedom is:

$$F^{(1)}_{exc,i}(\omega) = i\omega\rho \int_S (\Phi_I + \Phi_D) n_i dS, \tag{4}$$

where n_i is the normal vector component in the i-th direction, and S is the wetted surface from the ANSYS Aqwa mesh (maximum element size 2 m). The radiation forces yield the added mass and damping coefficient:

$$F_{R,i} = -\sum_{j=1}^{6} [A_{ij}\ddot{x}_j + B_{ij}\dot{x}_j], \tag{5}$$

where:

- $A_{ij} = -\frac{\rho}{\omega} Im[\int_S \Phi_{R,j}\, n_i dS]$ is the added mass coefficient.
- $B_{ij} = -\rho Re[\int_S \Phi_{R,j}\, n_i dS]$ is the radiation damping coefficient.

These coefficients are frequency-dependent and solved numerically using the BEM

doi:10.6342/NTU202500993

via the boundary integral equation:

$$c(\vec{r})\Phi(\vec{r}) + \int_s \Phi(\vec{y})\frac{\partial G(\vec{r},\vec{y})}{\partial n}dS = \int_s G(\vec{r},\vec{y})\frac{\partial \Phi(\vec{y})}{\partial n}dS, \tag{6}$$

where $G(\vec{r},\vec{y})$ is the Green's function satisfying the free-surface condition.

Second-Order Forces (Full QTF)

The full Quadratic Transfer Function (QTF) captures second-order forces from wave-wave interactions, computed as:

$$F^{(2)}_{exc,i}(t) = \sum_m \sum_n A_m A_n [T_i^+(\omega_m,\omega_n)e^{-i(\omega_m+\omega_n)t} + T_i^-(\omega_m,\omega_n)e^{-i(\omega_m+\omega_n)t}], \tag{7}$$

where:

- $T_i^+(\omega_m,\omega_n)$ is the sum-frequency QTF, contributing to high-frequency responses.
- $T_i^-(\omega_m,\omega_n)$ is the difference-frequency QTF, driving low-frequency motions like slow drift.
- A_m and A_n are wave amplitudes for frequencies ω_m and ω_n.

The QTFs are derived from the second-order potential $\Phi^{(2)}$, which satisfies $\nabla^2\Phi^{(2)} = 0$ with a forcing term on the free surface from quadratic products of the first-order potential (e.g., $\nabla\Phi^{(1)} \cdot \nabla\Phi^{(1)}$). OrcaWave computes these using perturbation theory, requiring additional BEM solutions and increasing computational demand due to

doi:10.6342/NTU202500993

the full QTF scope.

2.4.3 Wave Environment

OrcaWave simulates regular waves and irregular sea states via a JONSWAP spectrum, with the surface elevation given by:

$$\eta(t) = \sum_n A_n \cos(\omega_n t + \epsilon_n), \tag{8}$$

where $A_n = \sqrt{2S(\omega_n)\Delta\omega}$, $S(\omega)$ is the spectral density, ω_n is the n-th frequency component, ϵ_n is a random phase angle. The full QTF from Section 2.4.2 enhances accuracy for irregular waves by capturing nonlinear interactions across frequency pairs, critical for assessing resonant and slow-drift responses in shallow water.

2.5 Dynamic Simulation in OrcaFlex

OrcaFlex extends the hydrodynamic analysis from OrcaWave into the time domain, enabling a detailed simulation of the floating platform and its mooring system under combined environmental loads. This tool solves the nonlinear equations of motion for the FOWT system in six degrees of freedom (surge, sway, heave, roll, pitch, and yaw), capturing dynamic interactions critical to mooring tension and platform offset predictions. The established numerical model implemented in OrcaFlex is illustrated in Figure 7, and the corresponding theoretical framework and governing equations are detailed below.

doi:10.6342/NTU202500993

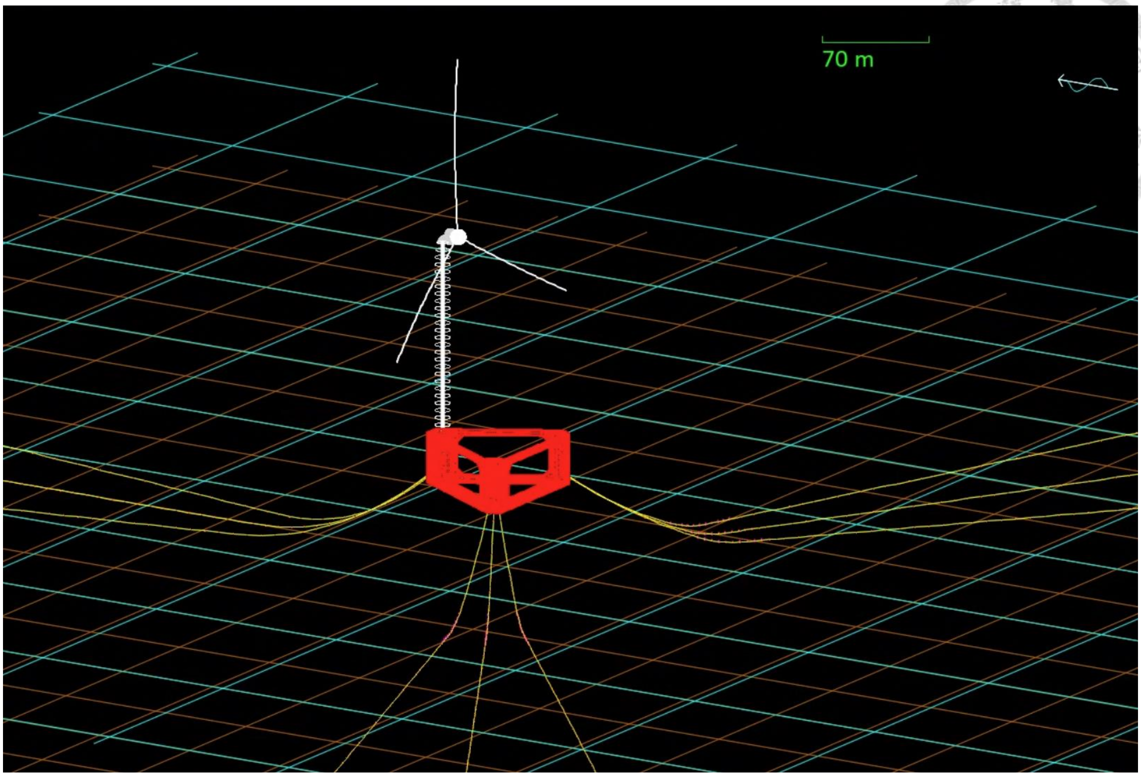

Figure 7: OrcaFlex Model of TaidaFloat FOWT and Mooring System

2.5.1 Equation of Motion

The dynamic motion of the gloating platform is governed by Newton's second law, formulated in vector form to account for its six degrees of freedom (surge, sway, heave, roll, pitch, yaw). The equation is expressed as:

$$\boldsymbol{M}\ddot{\vec{x}} + \boldsymbol{C}\dot{\vec{x}} + \boldsymbol{K}\vec{x} = \vec{F}_{hydro}(t) + \vec{F}_{moor}(t) + \vec{F}_{wind}(t) + \vec{F}_{current}(t), \tag{9}$$

where:

- $\boldsymbol{M}$ is the mass matrix, combining the structural mass of the floating platform (from ANSYS SpaceClaim) and the frequency-dependent added mass (A_{ij}) imported from OrcaWave's hydrodynamic database (HDB).

doi:10.6342/NTU202500993

- $\boldsymbol{C}$ is the damping matrix, incorporating radiation damping (B_{ij}) from OrcaWave and supplemental viscous damping (e.g., from drag forces).

- $\boldsymbol{K}$ is the stiffness matrix, representing hydrostatic restoring forces derived from the platform's buoyancy and geometry (e.g., based on the center of buoyancy calculated in SpaceClaim).

- $\vec{x} = (x_1, x_2, x_3, x_4, x_5, x_6)$, $\dot{\vec{x}}$, $\ddot{\vec{x}}$ are the displacement, velocity, and acceleration vectors, respectively, in the six degrees of freedom.

- $\vec{F}_{hydro}(t)$ is the time-varying hydrodynamic force vector from OrcaWave, detailed in Section 2.5.2.

- $\vec{F}_{moor}(t)$is the mooring force vector from the mooring systems, computed by the method in Section 2.5.3.

- $\vec{F}_{wind}(t), \vec{F}_{current}(t)$ are the wind and current load vectors, typically applied as external forces.

The mooring force $\vec{F}_{moor}(t)$ is derived from the nodal tension calculations of the lumped-mass model described in Section 2.5.3, reflecting the dynamics of the mooring systems. OrcaFlex solves this equation in the time domain using a numerical integration scheme, capturing the platform's transient response under combined environmental loads.

doi:10.6342/NTU202500993

2.5.2 Hydrodynamic Force

The hydrodynamic force vector $\vec{F}_{hydro}(t)$ acting on the floating platform includes both first-order and second-order contributions, reflecting the full quadratic transfer function (QTF) computed in OrcaWave. For the i-th degree of freedom, the force is:

$$\vec{F}_{hydro}(t) = F_{exc,i}^{(1)}(t) + F_{exc,i}^{(2)}(t) - \sum_j A_{ij}\ddot{x}_j(t) - \int_{-\infty}^{t} K_{ij}(t-\tau)\dot{x}_j(\tau)d\tau, \tag{10}$$

where:

- $F_{exc,i}^{(1)}(t)$ is the first-order excitation force, proportional to wave amplitude, derived from OrcaWave's linear wave theory outputs based on potential flow (Section 2.4.2).
- $F_{exc,i}^{(2)}(t)$ is the second-order excitation force, proportional to the square of wave amplitude, computed using the full QTF:

$$\begin{aligned} F_{exc,i}^{(2)}(t) = \sum_m \sum_n A_m A_n \, [T_i^{+}(\omega_m, \omega_n)\cos((\omega_m + \omega_n)t + \epsilon_m + \epsilon_n) + \\ [T_i^{-}(\omega_m, \omega_n)\cos((\omega_m - \omega_n)t + \epsilon_m - \epsilon_n), \end{aligned} \tag{11}$$

where T_i^{+} and T_i^{-} are the sum- and difference-frequency QTFs for the i-th degree of freedom, capturing high-frequency (e.g., resonant) and low-frequency (e.g., slow drift) responses, respectively; A_m and A_n are wave amplitudes; and ϵ_m and ϵ_n are phase angles.

- $\sum_j A_{ij}\ddot{x}_j(t)$ is the added mass force, accounting for the inertial contribution of the surrounding fluid, with A_{ij} from OrcaWave.

doi:10.6342/NTU202500993

- $\int_{-\infty}^{t} K_{ij}(t-\tau)\dot{x}_j(\tau)d\tau$ is the radiation force with memory effects, where $K_{ij}(t)$ is the retardation function, obtained via the inverse Fourier transform of the radiation damping $B_{ij}(\omega)$:

$$K_{ij}(t) = \frac{2}{\pi}\int_{0}^{\infty} B_{ij}(\omega)\cos(\omega t)d\omega. \tag{12}$$

This convolution integral ensures that past motions influence current forces, critical for modeling the floating platform's oscillatory behavior. For slender mooring elements, additional hydrodynamic forces are computed in Section 2.5.3 using Morison's equation, complementing the platform's potential flow-based loads and enhancing the overall dynamic analysis.

2.5.3 Mooring Line Dynamics

The mooring system consisting of catenary or taut lines is modeled in OrcaFlex using a finite element approach to capture its nonlinear dynamic behavior under environmental loads. Each mooring line is discretized into a series of lumped masses connected by springs, enabling the software to simulate complex interactions such as stretch, snap loads, and seabed contact. This lumped-mass model provides a balance between computational efficiency and physical accuracy, making it suitable for analyzing the tension and offset of the FOWT.

The dynamics of each mooring line segment are governed by the equation of motion

doi:10.6342/NTU202500993

for the i-th node:

$$m_i \ddot{\vec{r}}_i = \vec{T}_{i+1} - \vec{T}_i + \vec{F}_{hydro,i} + \vec{F}_{gravity,i} + \vec{F}_{buoyancy,i}, \tag{13}$$

where m_i and $\vec{r}_i$ are the mass and position vector of the i-th node, respectively, and $\ddot{\vec{r}}_i$ is its acceleration. The terms on the right-hand side represent the forces acting on the node, detailed as follows.

The net tension force, $\vec{T}_{i+1} - \vec{T}_i$, arises from the difference in tension between adjacent segments. The tension at the i-th node, $\vec{T}_i$, is calculated based on the axial stiffness and elongation of the spring connecting nodes i and $i+1$:

$$\vec{T}_i = EA \frac{|\vec{r}_{i+1} - \vec{r}_i| - L_0}{L_0} \frac{\vec{r}_{i+1} - \vec{r}_i}{|\vec{r}_{i+1} - \vec{r}_i|}, \tag{14}$$

where EA is the axial stiffness (product of Young's modulus and cross-sectional area), L_0 is the unstretched length of the segment, and $\vec{r}_{i+1} - \vec{r}_i$ is the vector between consecutive nodes. This formulation accounts for the nonlinear stretching behavior of materials like polyester, while the chain segments exhibit minimal elasticity but significant weight and drag effects.

The hydrodynamic force, $\vec{F}_{hydro,i}$, is computed using Morison's equation, which is well-suited for slender elements such as mooring lines:

$$\vec{F}_{hydro,i} = \rho C_a A \left(\dot{\vec{v}}_n - \ddot{\vec{r}}_i\right) + \frac{1}{2} \rho C_d D \left|\vec{v}_n - \dot{\vec{r}}_i\right| (\vec{v}_n - \dot{\vec{r}}_i), \tag{15}$$

where ρ is the water density, C_a and C_d are the added mass and drag coefficients, A

doi:10.6342/NTU202500993

is the cross-sectional area, D is the effective diameter, $\vec{v}_n$ is the normal component of the fluid velocity, and $\dot{\vec{r}}_i$ is the node's velocity. The first term represents the inertial force due to fluid acceleration (including added mass effects), while the second term captures viscous drag, which becomes significant during rapid motions or snap loads. These effects are critical for the chain-polyester-chain configuration, where the polyester's flexibility and the chain's weight influence dynamic responses differently.

The gravitational force, $\vec{F}_{gravity,i}$, and buoyant force, $\vec{F}_{buoyancy,i}$, are calculated for each node based on its submerged condition. The gravitational force is simply $m_i\vec{g}$, where $\vec{g}$ is the gravitational acceleration, adjusted for the line's material density. The buoyant force is

$$\vec{F}_{buoyancy,i} = -\rho V_i \vec{g}, \tag{16}$$

where V_i is the displaced volume of the segment, applied only to submerged portions. Seabed interaction is modeled with a contact stiffness and friction coefficient, allowing OrcaFlex to simulate the grounding of chain segments and its effect on tension distribution.

For a catenary mooring, the horizontal and vertical tension components can also be approximated using the catenary equation:

$$T = \sqrt{(\omega s)^2 + H^2}, \tag{17}$$

doi:10.6342/NTU202500993

where ω is the submerged weight per unit length, s is the suspended length, and H is the horizontal force component. This complements the lumped-mass model by providing an analytical check for static conditions. Nonlinear effects—such as line stretch, damping, and snap loads—are fully resolved in the time-domain simulation, ensuring accurate prediction of mooring tensions and platform offsets under dynamic wave, wind, and current loads.

2.5.4 Wind and Current Load

Wind loads on the turbine are calculated using a thrust coefficient (C_T), and wind speed (U_w), applied at the rotor hub:

$$F_{wind} = \frac{1}{2}\rho_{air}C_T A_{rotor} U_{hub}^2, \tag{18}$$

where ρ_{air} is air density and A_{rotor} is the rotor area. Current loads are modeled as steady drag forces on the submerged structure, using Morison's equation with appropriate coefficients. These loads are superimposed on the wave-induced forces to simulate realistic environmental conditions.

2.5.5 Blade-Pitch Controller and Generator-Torque Controller

To simulate operational conditions, OrcaFlex incorporates a blade-pitch controller and generator-torque controller. The blade-pitch controller adjusts the pitch angle (β) to regulate rotor speed and mitigate aerodynamic loads, typically following a proportional-

doi:10.6342/NTU202500993

integral (PI) control law:

$$\beta = K_p e + K_i \int e\, dt, \tag{19}$$

where e is the error between target and actual rotor speed, and K_p and K_i are controller gains. The generator-torque controller adjusts torque T_g to maintain power output, often using a quadratic relationship with rotor speed (Ω):

$$T_g = k\Omega^2, \tag{20}$$

where k is a constant tuned to the turbine's power curve. These controllers are implemented via external functions in OrcaFlex, ensuring realistic turbine behavior under varying wind speeds.

2.6 MPM Method for Mooring Tension

The inherent variability of ocean waves requires a statistical approach to mooring analysis to capture the stochastic nature of wave conditions. A conventional method, as described in Appendix A.2, computes the mean of maximum tensions from each simulation, yielding a conservative estimate that may overestimate the true extreme value due to its reliance on raw maxima [22]. In contrast, the Most Probable Maximum (MPM) method offers a robust statistical framework by modeling peak tension distributions and accounting for the probabilistic nature of extreme events. Aligned with DNV recommendations [22], this study employs the MPM method to estimate the most

doi:10.6342/NTU202500993

probable maximum tension in mooring lines, utilizing a 3-parameter Weibull distribution for peak tensions and a Gumbel distribution for extreme value estimation. The MPM methodology is implemented in a Python script, as detailed in Appendix B. This script uses the OrcFxAPI, which is a Python-based application programming interface (API) developed by Orcina for extracting and processing simulation data from OrcaFlex. These simulations generate time-series data for the effective tension of the mooring lines. The MPM methodology is detailed below, beginning with the peak extraction process.

2.6.1 Peak Extraction

The MPM method starts by extracting peak tension values from the time-series data of the mooring line exhibiting the highest tension. An up-crossing algorithm identifies peaks when the tension exceeds a threshold, defined as the mean tension plus four times the standard deviation:

$$T_{threshold} = \mu_T + 4 \cdot \sigma_T, \tag{21}$$

where μ_T is the mean tension and σ_T is the standard deviation of the time-series tension data. This threshold is set to avoid underestimating significant peaks, ensuring that only meaningful peaks are considered while filtering out noise and minor fluctuations. The algorithm evaluates peaks between consecutive up-crossings, as well as the first and last peaks in the time series, provided they exceed the threshold. Figure 8 illustrates the

doi:10.6342/NTU202500993

time-series data with identified peaks for one case in this study.

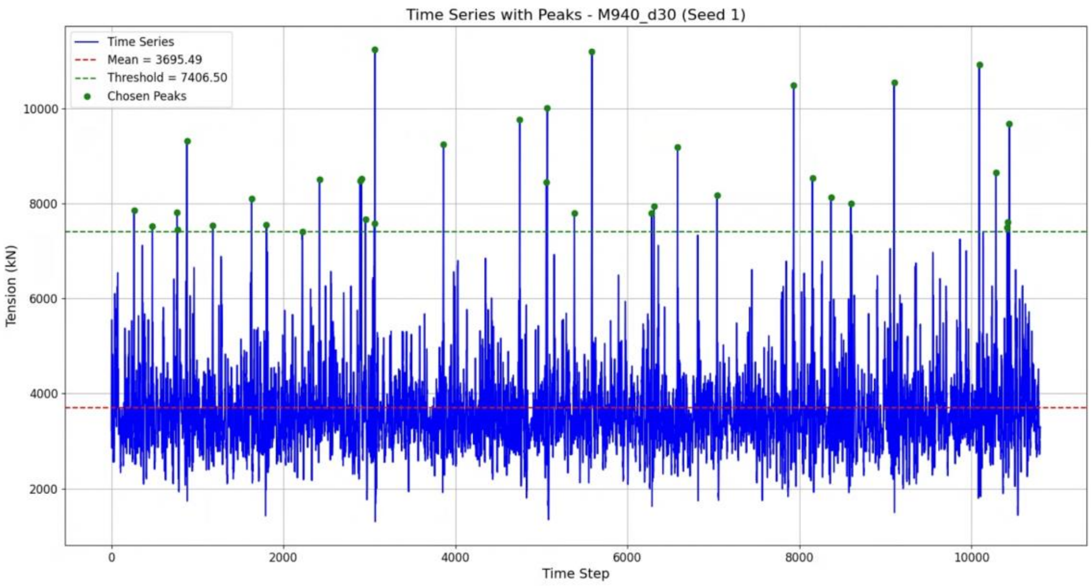

Figure 8: Time-Series Tension Data with Identified Peaks for a Selected Case.

2.6.2 Statistical Modeling and MPM Calculation

The extracted peak tensions are modeled using a 3-parameter Weibull distribution, characterized by shape (k), location (γ), and scale (λ) parameters, fitted via maximum likelihood estimation. Figure 9 presents the Weibull distribution fit for peak tensions in one case from this study. To estimate the extreme value distribution, n peak values (where n is the number of peaks in a simulation) are used to simulate 10,000 maxima, each representing the maximum of n random samples drawn from the fitted Weibull distribution.

doi:10.6342/NTU202500993

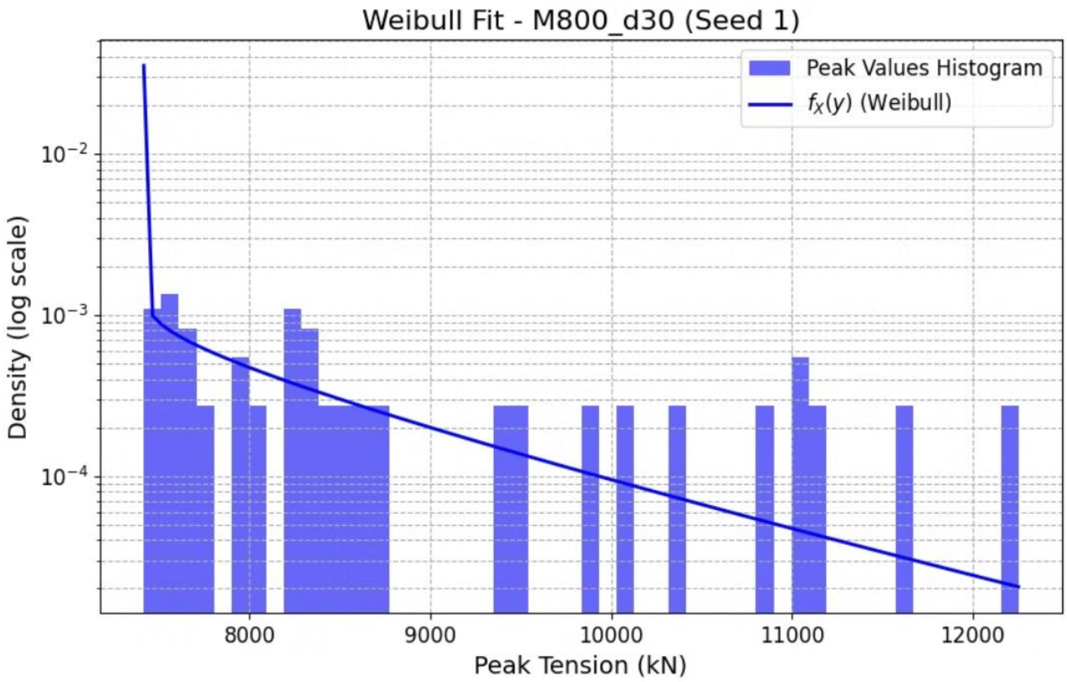

Figure 9: Weibull Distribution Fit for Peak Tensions in a Selected Case

These simulated maxima are fitted to a Gumbel distribution, characterized by location (μ), and scale (β)parameters. The MPM is calculated as the 37th percentile of the Gumbel distribution, representing the most probable maximum tension, as per DNV [22]. In this study, the MPM of each seed is capped at the maximum observed peak tension (seed maximum) in the simulation, preventing overestimation from unrealistic statistical predictions. The final MPM value is the mean of the MPM values calculated for each seed. Figure 10 shows the Gumbel fit of simulated maxima and the MPM estimation for one case in this study.

doi:10.6342/NTU202500993

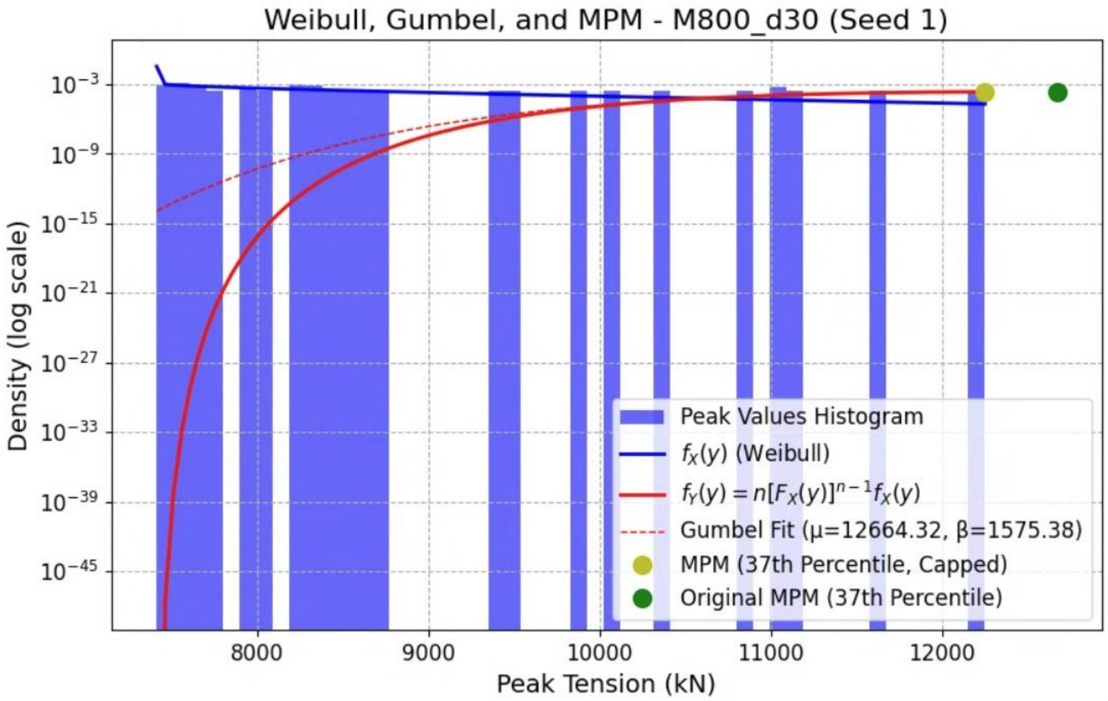

Figure 10: Gumbel Distribution Fit and MPM Estimation for a Selected Case

doi:10.6342/NTU202500993

3 Design Basis

3.1 Environmental Conditions

Taiwan is a region frequently impacted by typhoons, resulting in extreme wind, wave, and current conditions that pose significant challenges for the design of FOWTs. This study focuses on the environmental characteristics of the Taiwan Strait, with the target deployment site designated offshore of Hsinchu, Taiwan, as depicted in Figure 11.

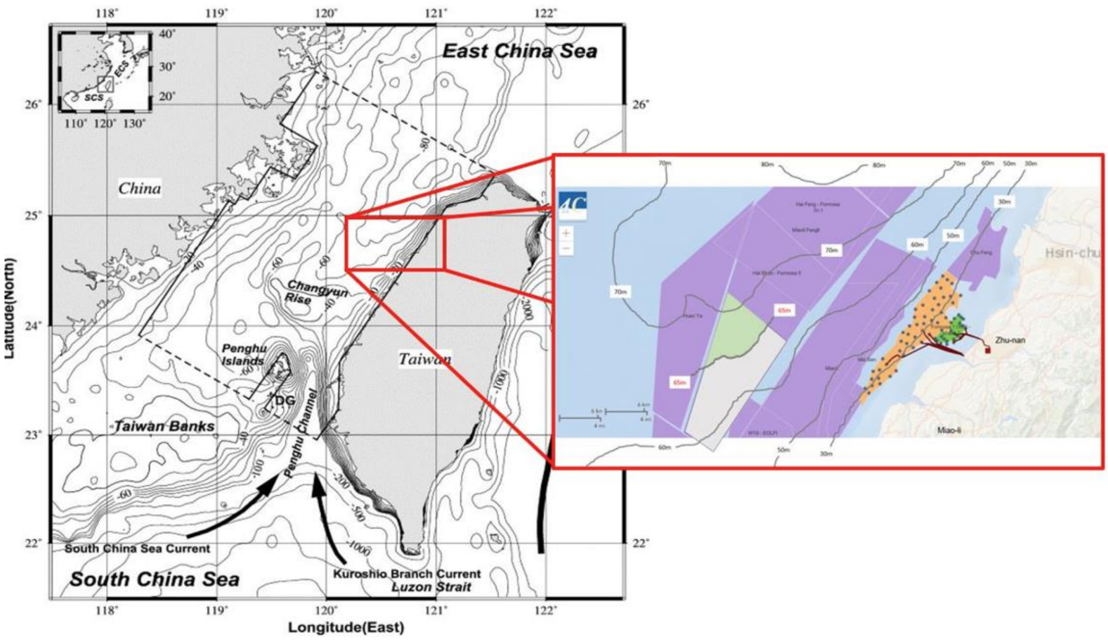

Figure 11: Assumed FOWT Deployment Site Offshore Hsinchu, Taiwan (Indicated by the Light Green Area) [23, 24]

According to the ABS rules [21], mooring system design under extreme conditions must account for Design Load Cases (DLC) 1.6 and 6.1, as outlined in Table 2Table 3. DLC 1.6 corresponds to the rated wind speed, where the FOWT experiences maximum wind thrust alongside significant wave and current forces. In contrast, DLC 6.1 represents

doi:10.6342/NTU202500993

the 50-year return period for combined wind, wave, and current conditions, explicitly addressing the extreme scenarios associated with typhoons. However, due to lack of wind and wave direction data, collinear extreme environmental conditions for wind, waves, and currents are assumed.

Table 2: Design Load Cases (DLC) Defined by ABS

	Wind	Waves	Wind and Wave Directionality	Sea Currents
DLC 1.6	$V_{rated\ wind\ speed}$	$H_{s,50-yr}$	MIS, MUL	50-yr Currents
DLC 6.1	$V_{10min,50-yr}$	$H_{s,50-yr}$	MIS, MUL	50-yr Currents

Previous research by Chen et al. [25], which utilized environmental data from the same offshore Hsinchu site as this study, conducted a mooring analysis and determined that both platform offset and maximum mooring tension were more severe under DLC 6.1 than DLC 1.6. Given that the focus of this study is to investigate mooring systems in typhoon-dominated environments, the analysis herein is limited to DLC 6.1, which specifically considers extreme typhoon conditions.

The environmental data for this study were sourced from the Central Weather Administration's offshore buoy near Hsinchu [26], supplemented by the National Oceanic and Atmospheric Administration's (NOAA) global ocean database [27], covering 11 years from 1997 to 2018. Statistical regression analysis was conducted by integrating these datasets to derive the 50-year return period values, which form the design and

doi:10.6342/NTU202500993

evaluation basis for the floating platform, with results presented in Table 3. Considering the characteristics of the target site, a water depth of 70 m was selected for the platform location. The 95% confidence level of the 50-year regression statistical extreme values yielded a maximum significant wave height (H_s) of 12.72 m, corresponding to a peak period (T_p) of 11.8 s, and an extreme ocean current of 1.59 m/s. For extreme wind speed, the 50-year regression statistical extreme value at a 95% confidence level was calculated as 53.47 m/s. However, to account for Taiwan's unique typhoon conditions, this study adopts the IEC-61400 standard's Class T wind speed of 57 m/s as the extreme wind speed value [28].

Table 3: 50-Year Return Period Environmental Data for Hsinchu Offshore Site

Taiwan Strait Hsinchu		
Water Depth	70 m	
DLC 6.1 (50-year return period)		
Wind	57 m/s	
Wave	H_s = 12.72 m	T_p = 11.8 s
Current	1.59 m/s	

3.2 Environment Setup

Simulations were performed using OrcaFlex, a dynamic analysis software for offshore systems, with input data from the specified simulation directory. To address the variability of irregular wave conditions, the analysis uses multiple wave seeds, each simulating a 3-hour storm, as required by classification societies. ABS [29] and American

doi:10.6342/NTU202500993

Petroleum Institute (API) [30] mandate at least 10 distinct wave seeds, while BV [31] specifies scaling factors based on the number of simulations and analysis method. DNV [22] recommends time-domain analysis with 10 to 20 seeds for robust statistical representation. This study employs 10 wave seeds, detailed in Table 4, meeting ABS, DNV and API minimum requirements while optimizing computational efficiency.

Table 4: Seed Values for Wave Spectrum Simulation in OrcaFlex

Simulation Duration	Build-up Time: 300 seconds Simulation Time: 10,800 seconds
	Number of Wave Seeds
Seed 1	111
Seed 2	222
Seed 3	333
Seed 4	444
Seed 5	555
Seed 6	666
Seed 7	777
Seed 8	888
Seed 9	999
Seed 10	1010

The environmental data utilized in the OrcaFlex simulation are detailed as follows:

- **Wind Conditions**: A 10,800-second time-series full-field dataset was generated using TurbSim and subsequently imported into OrcaFlex.
- **Wave Conditions**: A 10,800-second time-series JONSWAP spectrum was simulated directly in OrcaFlex, based on ten distinct seed values in Table 4. Due to space

doi:10.6342/NTU202500993

limitations, only the spectrum for Seed 1 is shown in Figure 12.

- **Current Conditions**: Modeled as steady.

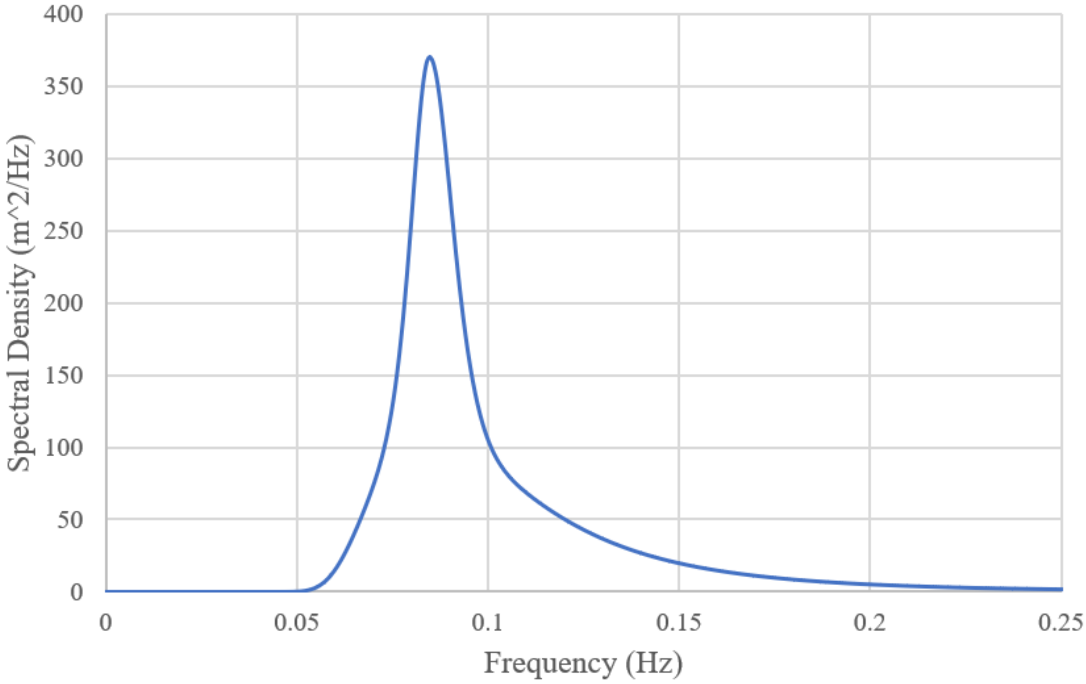

Figure 12: Example Wave Spectrum from OrcaFlex (Seed 1)

3.3 Mooring Chain

To withstand the harsh environmental conditions of the Taiwan Strait, this study employs an R4S-grade mooring chain, recognized for its exceptional strength and stiffness. Extensively validated in industrial applications, this grade is well-suited for demanding marine environments.

Corrosion is addressed by increasing the mooring chain's diameter with a corrosion allowance. Corrosion rates depend on site-specific factors, such as seawater temperature and dissolved inorganic nitrogen (DIN) levels. In the absence of detailed site-specific

doi:10.6342/NTU202500993

corrosion data for the Taiwan Strait, this study adopts reference values from the ABS [29]. Guo et al. [32] report a low DIN level for the region, corresponding to a corrosion rate of 0.2 mm/year to 0.4 mm/year, as classified by ABS [29]. For a conservative design, a corrosion rate of 0.4 mm/year—the upper limit—is selected. For an offshore wind farm with a 25-year operational lifespan, this results in a cumulative corrosion of 10 mm. Accordingly, a 10 mm corrosion allowance is incorporated into the chain diameter.

The largest mooring chain diameter currently used in industry, 170 mm, is selected for this study. After accounting for the 10 mm corrosion allowance, the effective chain diameter at the end of its service life is 160 mm.

The Minimum Breaking Load (MBL) for the R4S-grade mooring chain is calculated using the equation provided by Ma et al. [7], expressed as:

$$0.0304 \times d^2(44 - 0.08d), \tag{22}$$

where d is the chain diameter in millimeters.

For the 170 mm diameter chain, the MBL is 26,708 kN. At the end-of-life diameter of 160 mm, the MBL is reduced to 24,281 kN. The initial 170 mm diameter is used to determine the pre-tension level in the mooring analysis, while the end-of-life 160 mm diameter, with its corresponding MBL of 24,281 kN, serves as the benchmark for compliance with maximum tension design requirements in Section 6.1. The mooring

doi:10.6342/NTU202500993

chain parameters are summarized in Table 5.

Table 5: Specifications of the Selected Mooring Chain

Chain Grade	R4S
Chain Diameter / MBL (New)	170 mm / 26,708 kN
Chain Diameter / MBL (End of Life)	160 mm / 24,281 kN
Corrosion Rate	0.4 mm/year
Operation Lifespan	25 years

doi:10.6342/NTU202500993

4 Floating Offshore Wind Turbine System

This study employs the third-generation TaidaFloat, an optimized off-column hexagonal flat-plate semi-submersible, evolving from the earlier designs by Ivanov et al. [33] and Hsu et al. [34] to support an IEA 15 MW wind turbine [20]. Wu et al. [35] provides a comprehensive synthesis of TaidaFloat's design evolution, introducing the third-generation model and detailing the refinements and optimizations made over successive iterations.

4.1 TaidaFloat Platform Features

The left side of Figure 13 illustrates a conventional cylindrical-column semisubmersible, while the right side depicts TaidaFloat. Unlike traditional cylindrical curved-plate designs, TaidaFloat features three irregular hexagonal columns. All structural components are constructed from flat plates, representing a significant departure from conventional designs. This innovative approach enhances platform stability, improves material efficiency, and simplifies manufacturability.

The hexagonal flat-plate floating platform design offers several advantages, particularly by enabling 100% local production in Taiwan and significantly reducing manufacturing time. Conventional platforms consist of large-diameter cylindrical columns, which require large-scale bending machines. However, such machines are

doi:10.6342/NTU202500993

scarce and entail significant capital investment. In Taiwan, for example, no large bending machines are currently available to produce the large-diameter curved plates required for floating platform cylindrical columns.

In contrast, the use of flat plates eliminates the need for bending machines, allowing for more efficient welding through automatic or semi-automatic processes. Welding can be completed within a week, after which the platform is assembled at a dry dock. This streamlined approach significantly simplifies manufacturing and drastically shortens production time, enabling large-scale mass production.

Beyond its manufacturing advantages, the flat-plate design also enhances maintenance operations by providing a spacious, continuous platform surface for personnel. This improved accessibility facilitates the docking of maintenance vessels, increasing overall efficiency and functionality.

Figure 13: Comparison of a Conventional Semisubmersible (Left; [36], Courtesy of *Principle Power*) and TaidaFloat Platform (Right)

doi:10.6342/NTU202500993

4.2 General Properties of TaidaFloat System

The general properties of the TaidaFloat system are summarized in Table 6, including system mass, dimensions, centers of gravity (COG) and buoyancy (COB), and inertial properties. A detailed calculation of the COG and the load arrangement of TaidaFloat is provided in Table 7.

Table 6: The General Properties of Whole TaidaFloat System

Parameter	Units	Value
Total Displacement	t	21,028
Hull Steel Mass	t	4,974
RNA	t	991
Tower	t	1,260
Ballast Mass	t	13,802
Draft	m	20
Freeboard	m	14.75
COG_x (from SWL)	m	4.53
COG_y (from SWL)	m	0
COG_z (from SWL)	m	-2.425
COB_z (from SWL)	m	-12.99
Roll Inertia about Center of Gravity	$kg-m^2$	4.777E+10
Pitch Inertia about Center of Gravity	$kg-m^2$	5.111E+10
Yaw Inertia about Center of Gravity	$kg-m^2$	3.136E+10
Fairlead	3.75 m above keel	
Reference Origin	Pontoon centroid at SWL	

doi:10.6342/NTU202500993

Table 7: Stability Data and Load Arrangement of TaidaFloat

	Ballast (m)	Free Surface (t-m)	Mass (t)	COG_x (m)	COG_y (m)	COG_z (m)
Platform Mass			4,974	3.51	0	-8.17
Ballast (Side column 1)	8.28	161.7	1,372	-22.92	39.7	-12.11
Ballast (Side column 2)	8.28	161.7	1,372	-22.92	-39.7	-12.11
Ballast (Main column)	3.72	314.4	1,200	42.09	0	-14.39
Ballast (Pontoon)			9,858	0	0	-18.13
Tower			1,260	42.48	0	55.69
RNA			991	37.08	0	150
Total Mass / COG			21,028	4.53	0	-2.43
Displacement / COB (Design draft=20m)			21,028	4.53	0	-12.99
Trim (m)	0		KM (m)		40.465	
Roll (°)	0		KG (m)		17.575	
LCF (m)	9.13		GM (m)		22.891	
TPC (t)	6.54		GM_t (m)		14.932	
MTC (t-m)	58.85					

When installed, the platform has a draft of 20 m, with a 14.75-m freeboard extending to the upper deck of the columns. The fully assembled unit displaces 21,028 t of seawater (assuming a seawater density of 1,025 kg/m^3), comprising 4,974 t of platform structural steel, a 991-t RNA, a 1,263-t tower, and a 13,802-t permanent seawater ballast, which floods most of the three submerged pontoons and a portion of the columns. Since this study focuses on the design of the mooring system, the total displacement presented here will be updated to account for mooring vertical pretension.

Figure 14 presents the plan and elevation views and defines the coordinate system

doi:10.6342/NTU202500993

used in this study. The hull configuration consists of one larger-diameter column, referred to as the main column, and two smaller-diameter columns, referred to as side columns. The wind turbine tower is mounted atop the main column. The three columns are interconnected by three bottom pontoons measuring 10 m in width and 3.75 m in height, along with three 3.75-m square bracings attached to the bottom and top of the columns, respectively.

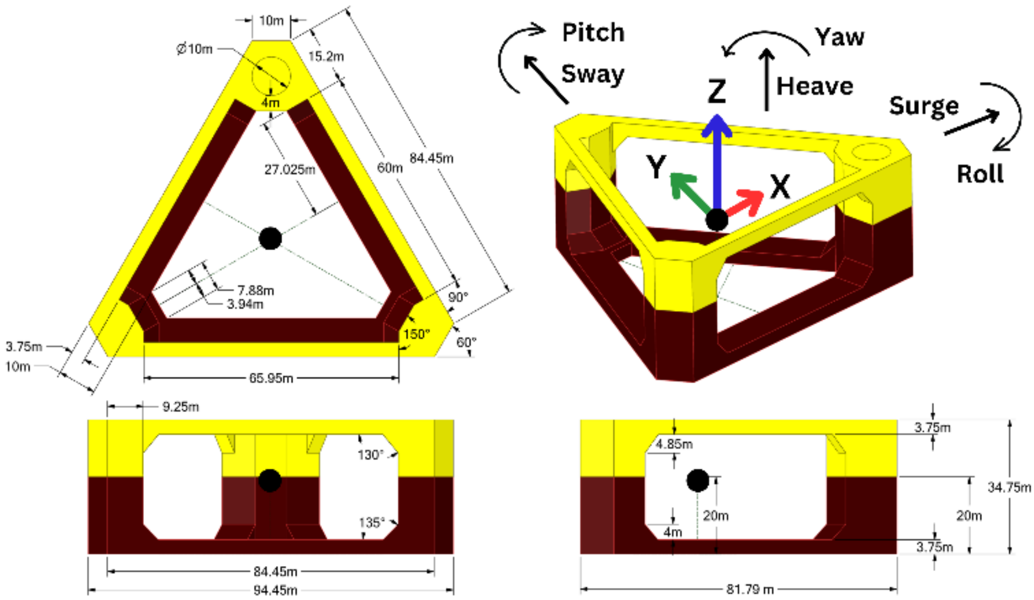

Figure 14: Dimensions of 15MW TaidaFloat Platform

4.3 Stability Analysis of TaidaFloat System

Stability is critical for the survivability of FOWTs, preventing capsizing and sinking under extreme conditions. For semi-submersible platforms like TaidaFloat, Classification Societies define two evaluation methods: the area-ratio-based method and the dynamic-response-based method, per ABS [21] and DNV [21, 37] standards. This thesis focuses

doi:10.6342/NTU202500993

on the area-ratio-based method to maintain thematic consistency, while Paper 1 in Appendix A.1 comprehensively details both methods.

The area-ratio-based analysis requires the wind heeling moment and righting moment curves. The righting moment is calculated using ORCA3D software for various inclination angles. The wind heeling moment, evaluated under a 50-year storm condition (wind speed: 57 m/s, as specified in Table 3, Section 3.1), is determined by:

$$M_{wind}(\theta) = \begin{cases} Max[M_{thrust}(\theta, V)] + (M_{pressure}{}^{V})cos^2\theta & ,\theta < \phi_C \\ M_{thrust}(\theta, V_{50-yr}) + (M_{pressure}{}^{V_{50-yr}})cos^2\theta & ,else \end{cases}, \quad (23)$$

where:

- M_{wind} = total wind heeling moment ($N \cdot m$)
- M_{thrust} = wind heeling moment induced by rotor thrust force ($N \cdot m$)
- $M_{pressure}$ = wind heeling moment induced by wind pressure force ($N \cdot m$)
- θ = inclination angle of the FOWT
- ϕ_C = turbine shutdown inclination angle

Per ABS [21] and DNV [21, 37], Area X+Y, as shown in Figure 16 (the area under the righting moment curve to the downflooding angle θ_d) must be at least 130% of Area Y+Z (the area under the wind heeling moment curve), expressed as:

$$\frac{Area\ X+Y}{Area\ Y+Z} \geq 1.3. \quad (24)$$

doi:10.6342/NTU202500993

A conservative $\theta_d = 17°$ was adopted in the preliminary design phase, as shown in Figure 15, corresponding to the point where the hull's main deck at the outer columns would submerge. As FOWTs are typically sealed structures, this constraint may be reconsidered in future designs.

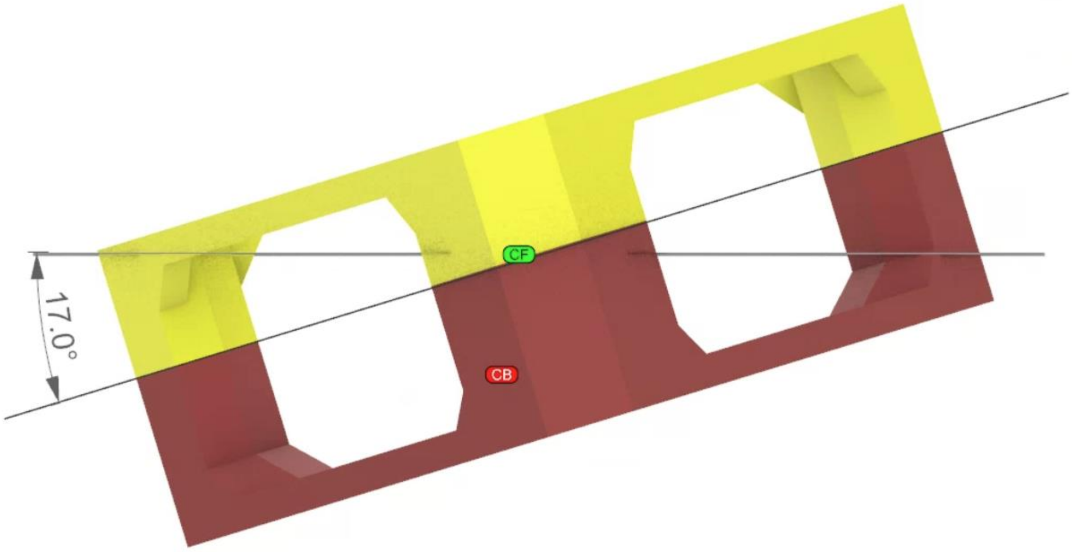

Figure 15: Downflooding Limit Angle of TaidaFloat Hull

Figure 16 illustrates the moment curves, with the equilibrium angle at $\theta_1 = 8.6°$ and the maximum inclination at $\theta_2 \cong 52°$. Table 8 indicates an area ratio of 1.31, slightly exceeding the minimum of 1.3, confirming that TaidaFloat meets ABS and DNV intact stability criteria for Taiwan Strait conditions.

doi:10.6342/NTU202500993

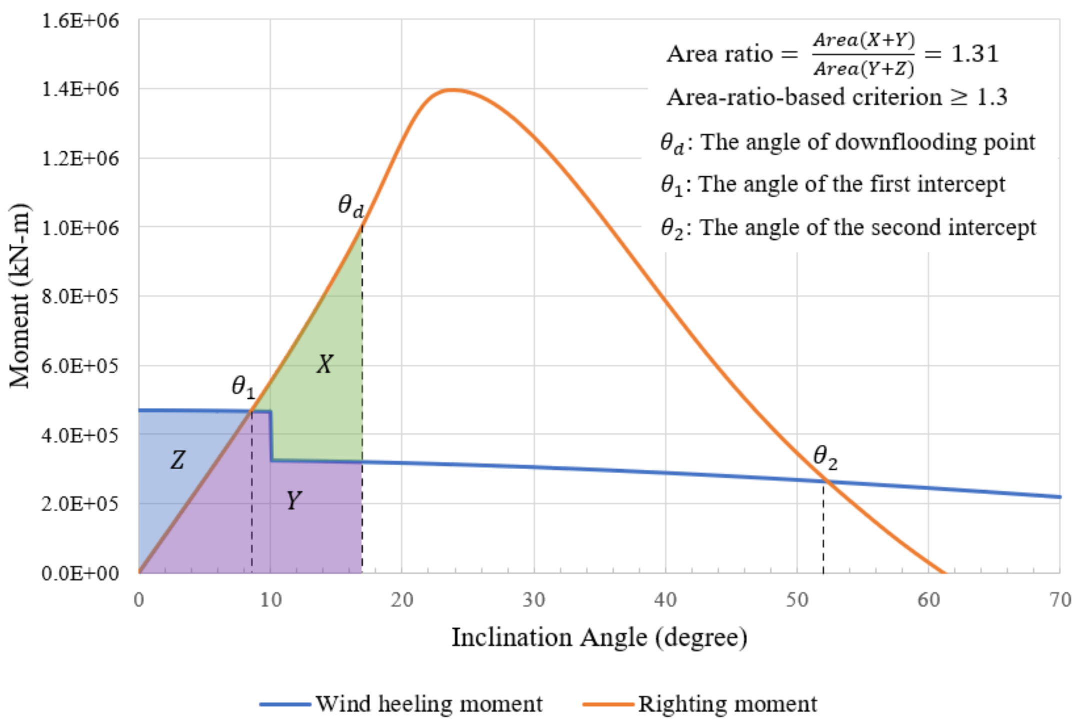

Figure 16: Stability Criteria Areas using Area-ratio-based Method for TaidaFloat

Table 8: Area-ratio-based Intact Stability Analysis Result

First intercept θ_1	8.6°
Second intercept θ_1	52°
Downflooding limit θ_d	17°
Area X+Y	9,130,214
Area Y+Z	6,970,976
Area ratio $\frac{\text{Area X+Y}}{\text{Area Y+Z}}$	1.31

4.4 Hydrostatic Properties of TaidaFloat System

The hydrostatic stiffness coefficients of the TaidaFloat system, derived from the submerged geometry of the platform, were computed using OrcaWave and validated against results from Aqwa. These coefficients, which represent the restoring forces and moments due to buoyancy and gravity, are summarized in Table 9. All values are

doi:10.6342/NTU202500993

expressed relative to the platform's reference origin, ensuring consistency with the coordinate system used throughout the analysis. The hydrostatic stiffness is a critical parameter in assessing the static stability of the semisubmersible, particularly under varying draft conditions.

Table 9: Hydrostatic Matix of TaidaFloat Evaluated by OrcaWave

	Heave	Roll	Pitch
Heave	6218.595	-208.6215e-6	-58.5068e3
Roll	-208.6212e-6	3.0373e6	-27.9364
Putch	-58.5068e3	-27.9364	5.2111e6

4.5 Hydrodynamic Properties of TaidaFloat System

The hydrodynamic properties of the TaidaFloat system, which dictate its response to wave forces, are characterized by response amplitude operators (RAOs) and related dynamic effects. RAOs, evaluated using OrcaWave and validated with Aqwa, quantify the platform's motion amplitude per unit wave amplitude across various frequencies and directions. To support comprehensive OrcaFlex simulations, RAOs were calculated for 12 wave headings from 0° to 330° at 30° intervals, relative to the platform's reference origin. Due to space constraints, only the results for a wave heading of 0° are presented here.

In the OrcaWave simulations, additional damping was incorporated to account for

doi:10.6342/NTU202500993

viscous effects and other energy dissipation mechanisms not fully captured by potential flow theory. Without this adjustment, the model would underestimate the damping of the system's motions, potentially overpredicting RAO peak amplitudes and leading to unrealistic response estimates. The additional damping values adopted in this study are 3% of the critical damping for heave, 2% of the critical damping for roll, and 2% of the critical damping for pitch of the TaidaFloat system, as presented in Table 10.

Given the current lack of experimental data for the TaidaFloat, these values were determined by referencing the RAOs of the IEA VolturnUS, a comparable 15 MW wind turbine semisubmersible with a three-column design. The additional damping was tuned to align the TaidaFloat's RAO peak values with those of the VolturnUS, ensuring a realistic representation of its hydrodynamic behavior.

Table 10: Additional Damping Coefficients for TaidaFloat in OrcaWave Hydrodynamic Diffraction Analysis

Degree of Freedom	Critical Damping	Additional Damping	
		Value	% of Critical Damping
Heave	1.120E5 kN/(m/s)	3.357E3 kN/(m/s)	3%
Roll	8.729E7 kN-m/(rad/s)	1.746E6 kN-m/(rad/s)	2%
Pitch	1.165E8 kN-m/(rad/s)	2.329E6 kN-m/(rad/s)	2%

For a wave heading of 0°, the analysis focused on RAOs for surge, heave, and pitch, as shown in Figure 17, Figure 18, and Figure 19, respectively. The TaidaFloat system

doi:10.6342/NTU202500993

exhibits symmetry about the x-axis (see Figure 14, Section 4.2), leading to zero net forces or moments in sway, roll, and yaw for wave headings of 0° or 180°. Consequently, the RAOs for these degrees of freedom (DOFs) are zero across all wave frequencies in this configuration. Beyond RAOs, the system's hydrodynamic behavior is shaped by added mass and damping effects, which are embedded in the numerical models and critical for understanding its stability under wave loading.

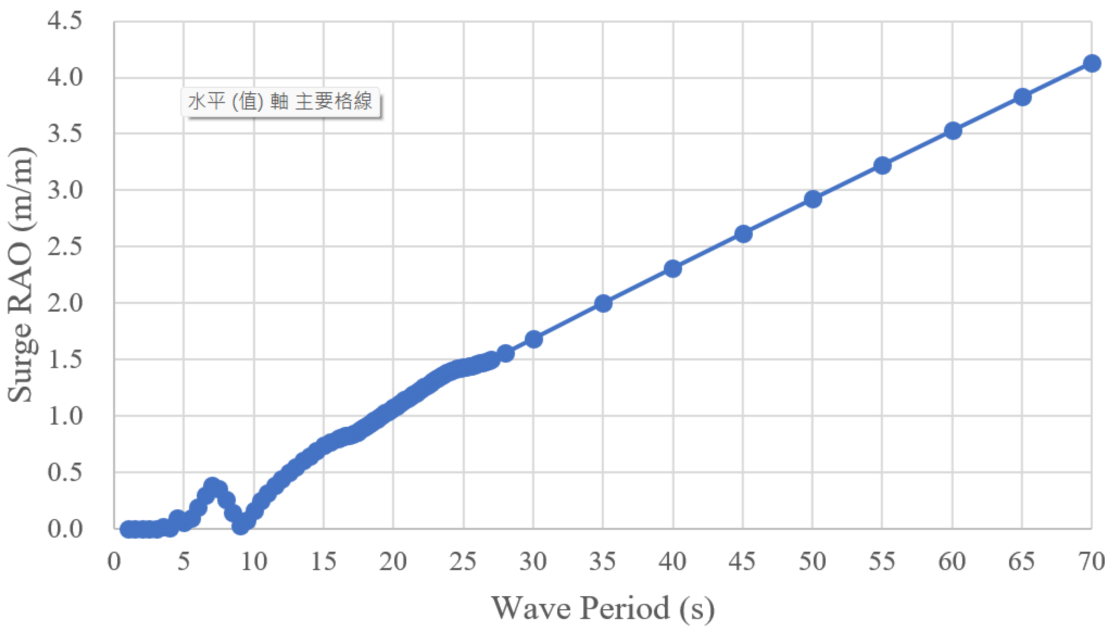

Figure 17: RAO for Surge Motion of TaidaFloat at 0° Wave Heading

doi:10.6342/NTU202500993

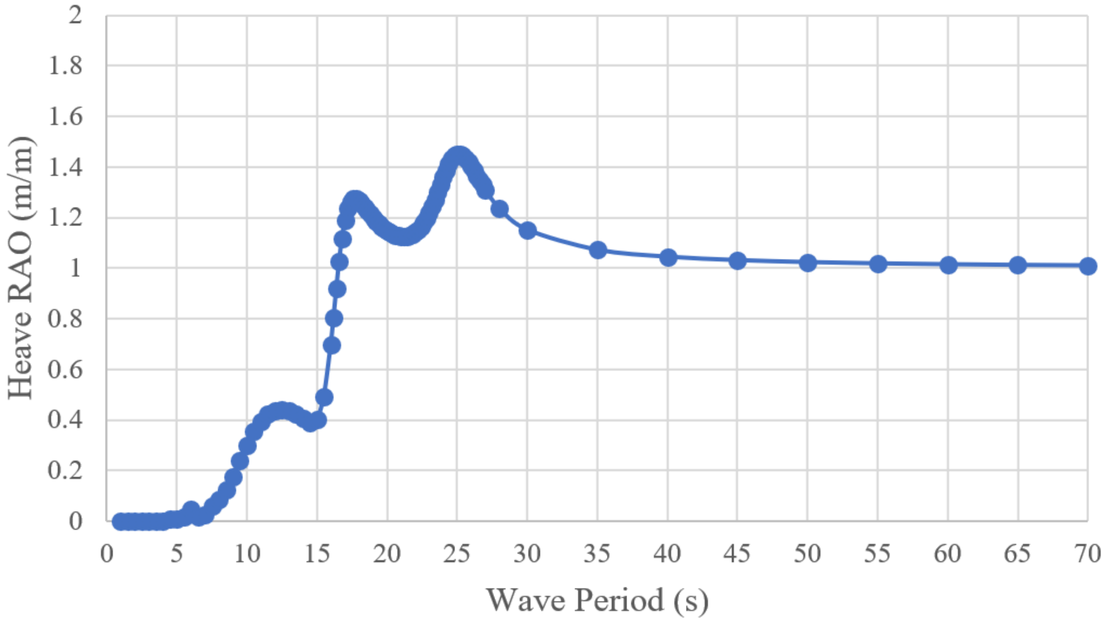

Figure 18: RAO for Heave Motion of TaidaFloat at 0° Wave Heading

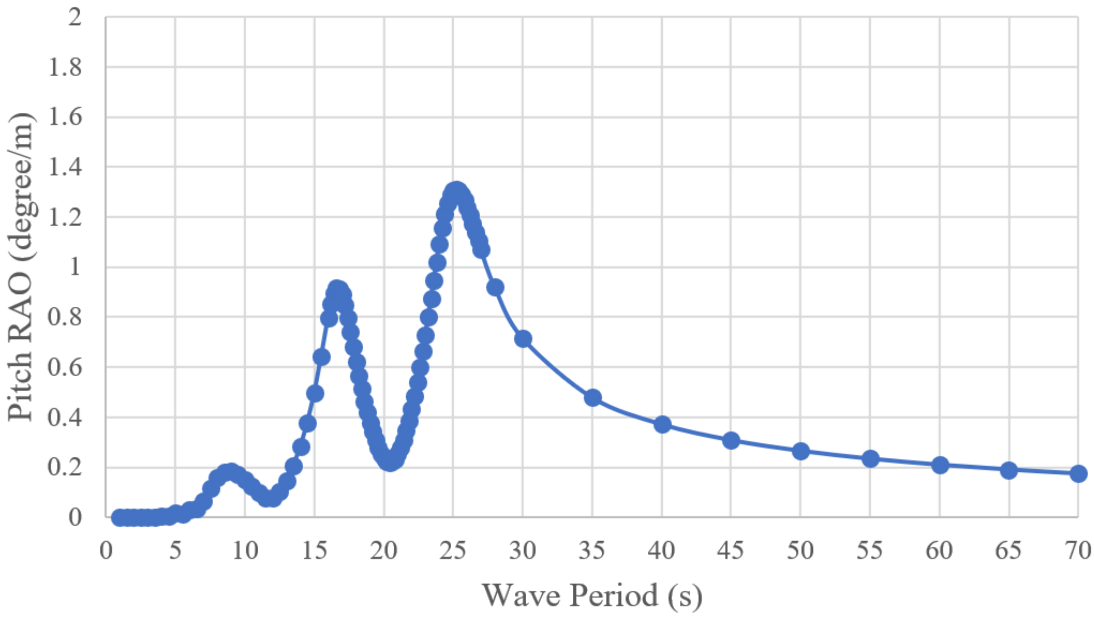

Figure 19: RAO for Pitch Motion of TaidaFloat at 0° Wave Heading

4.6 Drag Coefficients of TaidaFloat

The drag coefficients for TaidaFloat were determined through computational fluid dynamics (CFD) simulations conducted using Star-CCM+ by Professor Shiu-Wu Chao's

doi:10.6342/NTU202500993

research team. The analysis covered seven orientations, ranging from 0° to 180° at 30° intervals. The waterline served as the dividing plane: drag coefficients below the waterline were used to calculate current loads, as presented in Table 11, while those above the waterline were used to compute wind loads, as shown in Table 12. Additionally, Table 13 provides the area and area moment data necessary for calculating both current and wind loads.

Table 11: Drag Coefficients Below Waterline for Current Load Calculation

Direction	Surge	Sway	Heave	Roll	Pitch	Yaw
0°	-0.87	0.02	-0.27	0.01	0.23	0
30°	-0.6	1.01	-0.14	0.46	0.18	0.11
60°	-0.62	1.5	-0.47	0.68	0.03	0.16
90°	-0.31	1.5	-0.2	0.68	0.03	0.16
120°	0.46	1.13	-0.5	0.51	-0.43	0.12
150°	0.94	0.19	-0.13	0.09	-0.46	0.02
180°	1.3	0.01	-0.37	0	-0.72	0

Table 12: Drag Coefficients Above Waterline for Wind Load Calculation

Direction	Surge	Sway	Heave	Roll	Pitch	Yaw
0°	-1.4	0.04	0.38	-0.03	-0.95	0
30°	-1.1	1.63	0.3	-1.24	-0.75	0.04
60°	-0.87	2.29	0.42	-1.74	-0.57	0.05
90°	-0.45	2.24	0.35	-1.69	-0.28	0.05
120°	0.76	1.73	0.38	-1.31	0.62	0.04
150°	1.59	0.59	0.25	-0.45	1.19	0.01
180°	1.93	0.22	0.44	-0.17	1.47	0.01

doi:10.6342/NTU202500993

Table 13: Area and Area Moment for Current and Wind Load Calculations

	Surge area (m^2)	Sway area (m^2)	Heave area (m^2)	Roll area moment (m^3)	Pitch area moment (m^3)	Yaw area moment (m^3)	Load origin (x, y, z)
Current	1,225.9	872	2,557	1.74e4	2.45e4	1.36e5	0, 0, -11
Wind	944.0	689	1,332	1.04e4	1.42e4	6.23e4	0,0, 8.25

doi:10.6342/NTU202500993

5 Model Validation

Before conducting the mooring analysis of TaidaFloat in OrcaFlex, it is essential to establish the reliability of the numerical model through validation against experimental data. As experimental data for the 15 MW TaidaFloat configuration are currently unavailable, this study utilizes experimental results from the 5 MW TaidaFloat_Medium—a scaled-down design based on the 15 MW TaidaFloat—for model validation. The dimensions of TaidaFloat_Medium are presented in Figure 20. While its configuration and pontoon dimensions are nearly identical to those of TaidaFloat, the primary difference lies in the column size, with TaidaFloat_Medium featuring significantly smaller columns.

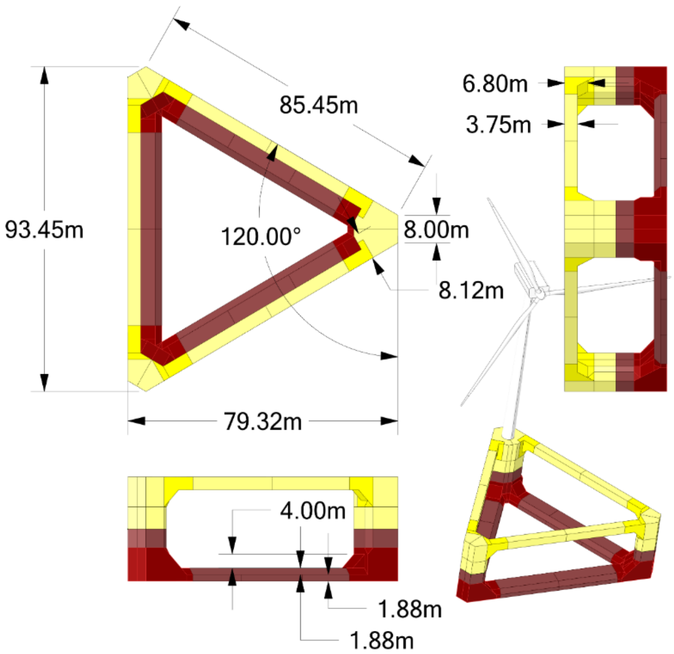

Figure 20: Geometry and Dimensions of TaidaFloat_Medium

The experimental data for TaidaFloat_Medium were obtained from 1:100 scale

doi:10.6342/NTU202500993

model tank tests conducted by Prof. Lin's team from National Taiwan University. In this study, the hydrodynamic numerical model was developed using OrcaWave's diffraction analysis. The simulated results were then compared with the experimental data to assess the accuracy and reliability of the model.

Figure 21 presents a comparison of the 1st-order surge load Response Amplitude Operator (RAO) for TaidaFloat_Medium. The diffraction analysis results closely align with the experimental data, although the experimental values are slightly lower than those from the simulation. This discrepancy can be attributed to external factors in the experimental setup, such as friction, which are expected to reduce the measured surge response compared to the idealized numerical predictions. Overall, the high degree of agreement between the experimental and diffraction analysis results confirms the accuracy and reliability of the methodology and settings employed in OrcaWave for this study.

Additionally, Figure 21 illustrates that the 1st-order surge load RAO of TaidaFloat follows a similar trend to that of TaidaFloat_Medium, reflecting the nearly identical configurations of the 15 MW TaidaFloat and the 5 MW TaidaFloat_Medium. However, the RAO values for TaidaFloat are higher, which is expected due to the larger column diameter of TaidaFloat. Under identical wave conditions, the smaller columns of

doi:10.6342/NTU202500993

TaidaFloat_Medium result in a reduced 1st-order surge load compared to TaidaFloat.

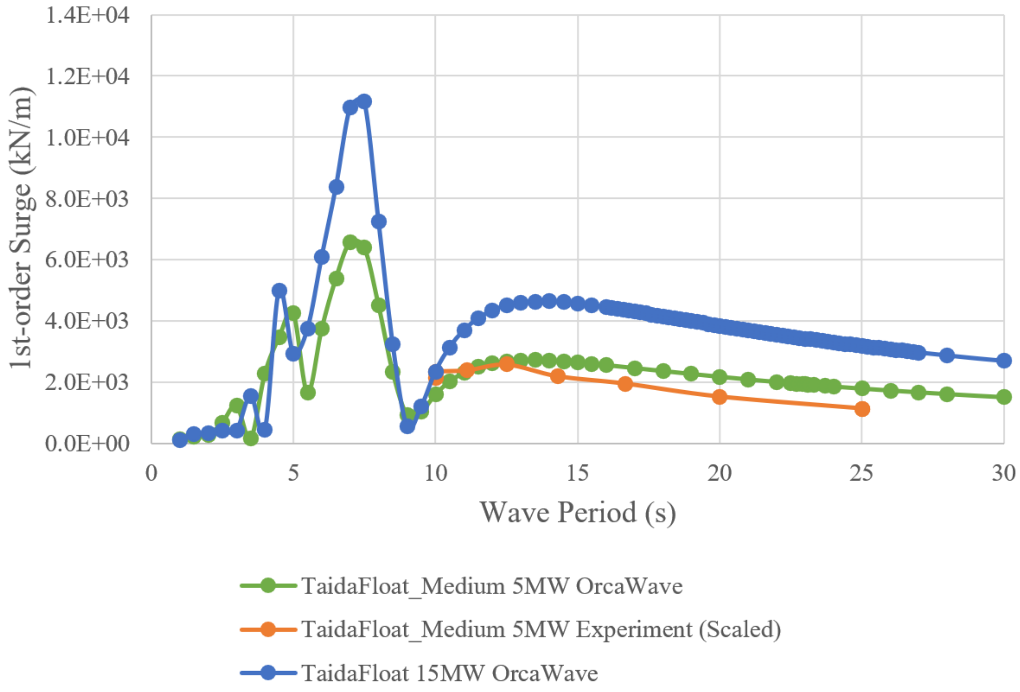

Figure 21: Comparison of 1st-Order Surge Load RAO: Experimental Data vs. OrcaWave Simulation for TaidaFloat_Medium and TaidaFloat

Similarly, Figure 22 compares the 1st-order heave load RAO for TaidaFloat_Medium. The diffraction analysis results exhibit strong consistency with the experimental data, though the experimental values are again slightly lower, likely due to frictional effects and other external forces in the tank setup that dampen the measured response. This minor deviation is anticipated, and the overall close correspondence between the experimental and simulated results further validates the accuracy and reliability of the OrcaWave diffraction analysis methodology employed in this study.

From Figure 22, it is evident that the 1st-order heave load RAO of TaidaFloat shares a similar trend with that of TaidaFloat_Medium, owing to their comparable configurations.

doi:10.6342/NTU202500993

However, unlike the surge load RAO—where TaidaFloat consistently exhibits higher values—the 1st-order heave load RAO behavior differs across wave periods. Before a 17-second period, TaidaFloat_Medium's RAO is slightly higher due to its smaller columns, which reduce hydrostatic stiffness and damping, enhancing its response to shorter waves despite a smaller diffraction force. After a 17-second period, TaidaFloat's RAO surges much higher because its larger columns generate a significantly greater diffraction force in long waves, dominating the response as inertial and damping effects diminish. These period-dependent differences highlight how column size influences heave dynamics under varying wave conditions.

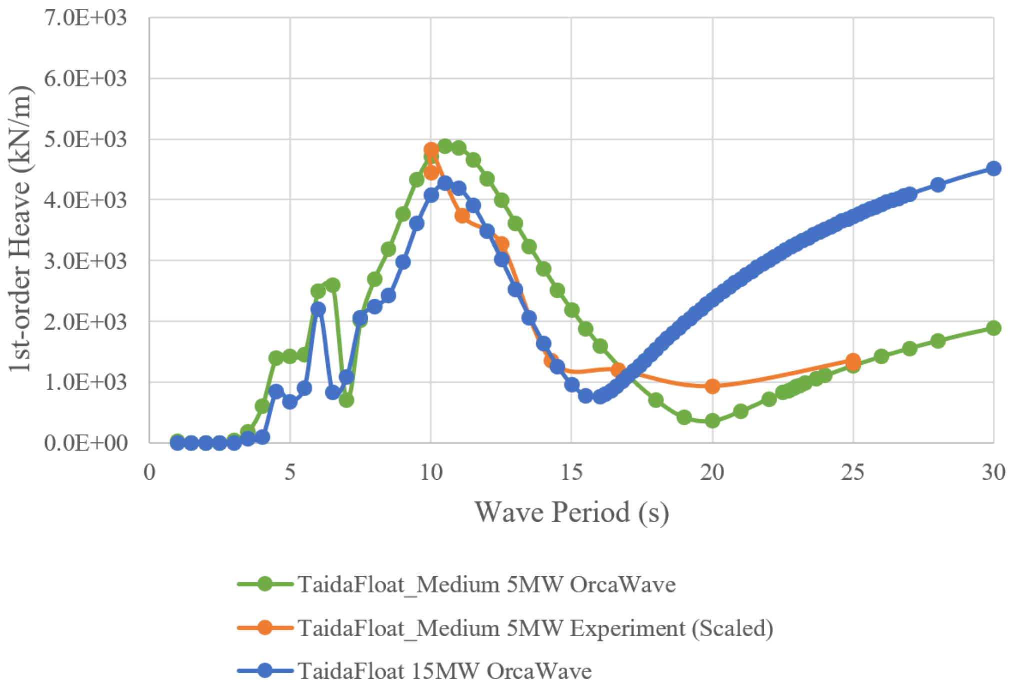

Figure 22: Comparison of 1st-Order Heave Load RAO: Experimental Data vs. OrcaWave Simulation for TaidaFloat_Medium and TaidaFloat

The model validation process confirms that the OrcaWave diffraction analysis

doi:10.6342/NTU202500993

methodology accurately predicts the hydrodynamic behavior of semisubmersible platforms, as demonstrated by the close agreement between simulated and experimental results for TaidaFloat_Medium. For both the 1st-order surge and heave load RAOs, the numerical model effectively captures the trends observed in the 1:100 scale tank tests conducted by Prof. Lin's team, with minor discrepancies attributed to experimental factors such as friction. These findings validate the reliability of the model settings and methodology. Although direct experimental data for the 15 MW TaidaFloat are unavailable, the consistent trends observed between TaidaFloat and TaidaFloat_Medium reinforce the model's applicability. This validation provides a solid foundation for the subsequent mooring analysis of TaidaFloat in OrcaFlex.

doi:10.6342/NTU202500993

6 Design Requirements

6.1 Maximum Mooring Line Tension

According to ABS regulations, the required safety factor for an intact mooring system is 1.67, while for a single-line damage scenario, the safety factor is 1.05. In this study, the maximum tension is determined using the Most Probable Maximum (MPM) approach, an extreme value statistic commonly employed in the offshore industry. Details of the MPM approach applied in this study are presented in Section 2.6. The safety factor is defined as:

$$Safety\ Factor = \frac{Minimum\ Breaking\ Load\ (MBL)}{Max.Mooring\ Line\ Tension}, \tag{25}$$

As detailed in Section 3.3, the MBL for the end-of-life 160 mm R4S-grade mooring chain is 24,281 kN. For an intact mooring system with a safety factor of 1.67, the maximum allowable mooring line tension is calculated as:

$$Max. mooring\ line\ tension = \frac{MBL}{Safety\ Factor} = \frac{24{,}281\ kN}{1.67} \approx 14{,}539kN, \tag{26}$$

This value of 14,539 kN serves as the design criterion for the intact mooring system in subsequent sections. If the maximum tension in any mooring line exceeds 14,539 kN, the design does not comply with ABS regulations.

6.2 Maximum Floater Offset

The maximum allowable floater offset is set at approximately 30% of the water depth

doi:10.6342/NTU202500993

(21m) to ensure that the FOWT's dynamic cable operates within its design bending radius limitations. The maximum floater offset in this study is defined as:

$$Offset = \sqrt{(Offset_x)^2 + (Offset_y)^2}, \tag{27}$$

doi:10.6342/NTU202500993

7 All-Chain Mooring System Design

This chapter outlines the design and optimization of a 3×3 all-chain mooring system for TaidaFloat FOWT, using the mooring configuration specified in TaidaFloat's ABS Approval in Principle (AIP) mooring analysis report [25, 38] as the baseline. Section 7.1 details the baseline all-chain mooring configuration. Section 7.2 analyzes critical environmental load directions using the baseline configuration to support subsequent optimization. Section 7.3 evaluates whether the baseline all-chain mooring design satisfies the design requirements specified in Chapter 6. Section 7.4 optimizes the mooring configuration by adjusting pre-tension and anchor radius to meet these standards.

7.1 Baseline All-Chain Mooring Configuration

The baseline all-chain mooring configuration, as specified in TaidaFloat's ABS AIP mooring analysis report [38], adopts a 3×3 mooring layout with an anchor radius of 840 m (12 times the water depth). Each mooring line is 795 m long, with a spread angle of 10 degrees between lines within the same cluster. The configuration details are provided in Table 14. The mooring layout, including numbered mooring lines, is illustrated in Figure 23. These mooring line numbers are used consistently throughout this thesis.

doi:10.6342/NTU202500993

Table 14: Parameters of Baseline All-Chain Mooring Configuration

Mooring Type	All chain (studless)
Mooring Pattern	3x3 (Three lines on each column)
Anchor Radius	840 m (12 times water depth)
Mooring line length	796 m
Mooring Line Spread Angle	10° between lines within the same cluster
Corrosion Allowance	0.4 mm per year
Chain Diameter (new)	170 mm
Chain Diameter (end of life)	160 mm
Chain Grade	R4S
Minimum Breaking Load (new)	26,708 kN
Minimum Breaking Load (end of life)	24,281 kN
Pre-tension	2,436 kN (9.1% MBL)
In Air Weight (new)	504 kg/m
In Water Weight (new)	575 kg/m
Axial Stiffness of Chain (new)	2.468e6 kN
Drag Coefficients (Normal, Tangential)	2.4, 1.15
Added Mass Coefficients (Normal, Tangential)	2.0, 1.0
Clump Weights	None

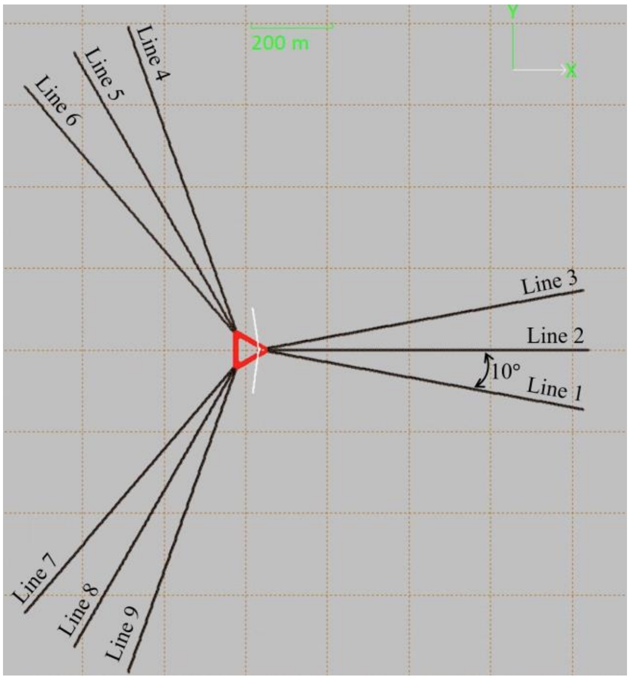

Figure 23: Baseline All-Chain Mooring Layout with Line Numbers

doi:10.6342/NTU202500993

7.2 Critical Environmental Load Directions for All-Chain Mooring Design

To streamline the design process, identifying critical environmental load directions is essential to avoid simulating all possible directions at every design stage. By focusing on critical directions, the mooring system analysis can be optimized, saving computational resources.

This study investigates the impact of extreme wind, wave, and current conditions during typhoons in the Taiwan Strait on FOWTs, focusing on Design Load Case (DLC) 6.1 from Table 2 in Section 3.1. Collinear extreme environmental conditions for wind, waves, and currents are assumed. Using the baseline all-chain mooring configuration, simulations were conducted at 15° intervals from 0° to 180° for collinear environmental load directions, as shown in Figure 24. Due to the symmetrical FOWT design, results from 180° to 360° are mirrored. This approach identifies the critical load directions of maximum mooring tension and platform offset, enabling a more efficient design process.

doi:10.6342/NTU202500993

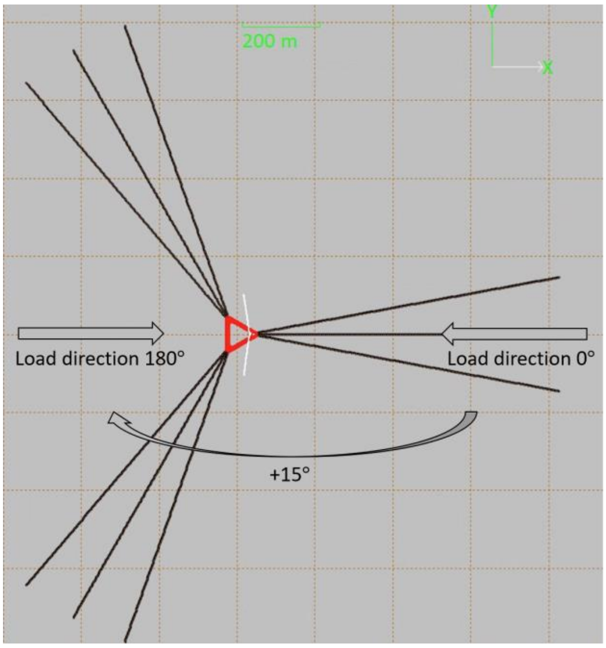

Figure 24: Environmental Load Directions for Mooring Simulations (0° to 180°)

7.2.1 Critical Directions for Maximum Mooring Tension

Analysis of various seeds revealed consistent trends, so only results from seed 111 are presented in Figure 25, illustrating the relationship between environmental load directions and maximum mooring line tension. When loads are applied from the 120° and 240° directions, Line 7 and Line 6 experiences the highest tension, indicating that these are the critical directions for maximum mooring tension.

This finding differs from prior studies. For instance, Chen et al. [25] identified 0° as the critical direction for maximum mooring tension in a 15MW TaidaFloat mooring system, and Chen et al. [39] assumed 0° for a 15MW center-column semi-submersible. 造成的原因將於 Section 7.2.2 進行分析說明。The critical directions of 120° and 240° in this study are attributed to the off-column design of TaidaFloat. Subsequent mooring

doi:10.6342/NTU202500993

design analyses in this study focus on the 120° environmental load direction.

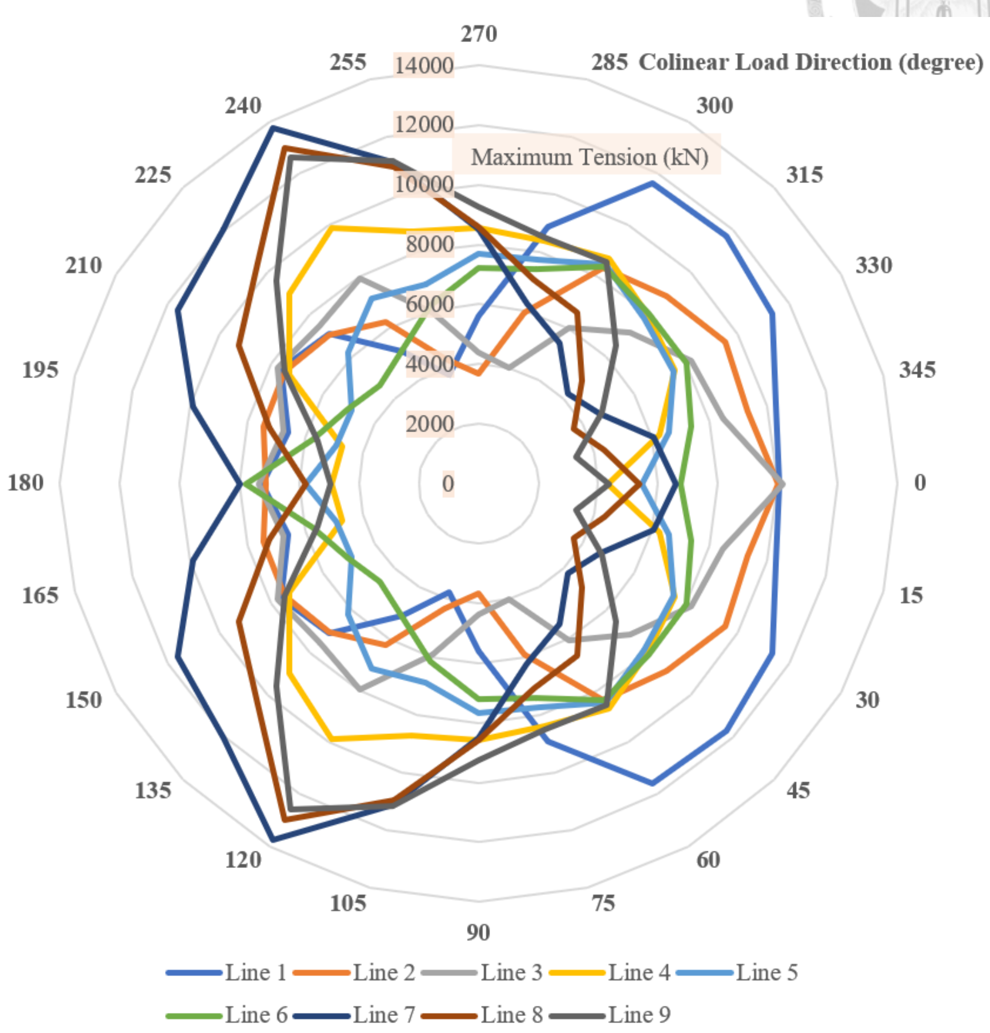

Figure 25: Maximum Mooring Line Tension vs. Environmental Load Directions for Baseline All-Chain Mooring Design (Seed 111)

7.2.2 Impact of Platform Design on Yaw Rotation and Mooring Line Tension

The off-column semi-submersible's non-symmetrical structure generates a yaw moment when turbine wind forces misalign with the main column causing platform rotation. This creates imbalanced loading across the mooring line cluster with excessive

doi:10.6342/NTU202500993

tension in one line. Aligning the main column with the wind reduces yaw in consistent wind conditions. In the Taiwan Strait's typhoon-prone environment multidirectional extreme loads trigger pronounced yaw rotation and concentrated tension posing major mooring design challenges. Conversely center-column semi-submersibles with a symmetrical layout and centrally placed turbine promote uniform load distribution and lower mooring line tensions.

Figure 26 illustrates the static simulation results for the TaidaFloat off-column platform under a 120° load direction. The blue solid line represents the 120° load direction mesh, while the black solid lines depict the mooring lines. The yellow box highlights mooring line Line 8, which deviates from the blue line due to platform yaw rotation. This yaw-induced uneven load distribution is evident in the suspended segments of mooring lines Line 7, 8, and 9. For clarity, a yellow dashed line distinguishes the suspended mooring line segments from those in contact with the seabed. Line 7 exhibits the longest suspended segment, indicating that yaw rotation lifts Line 7 from its resting position on the seabed, resulting in the highest tension among the mooring lines.

doi:10.6342/NTU202500993

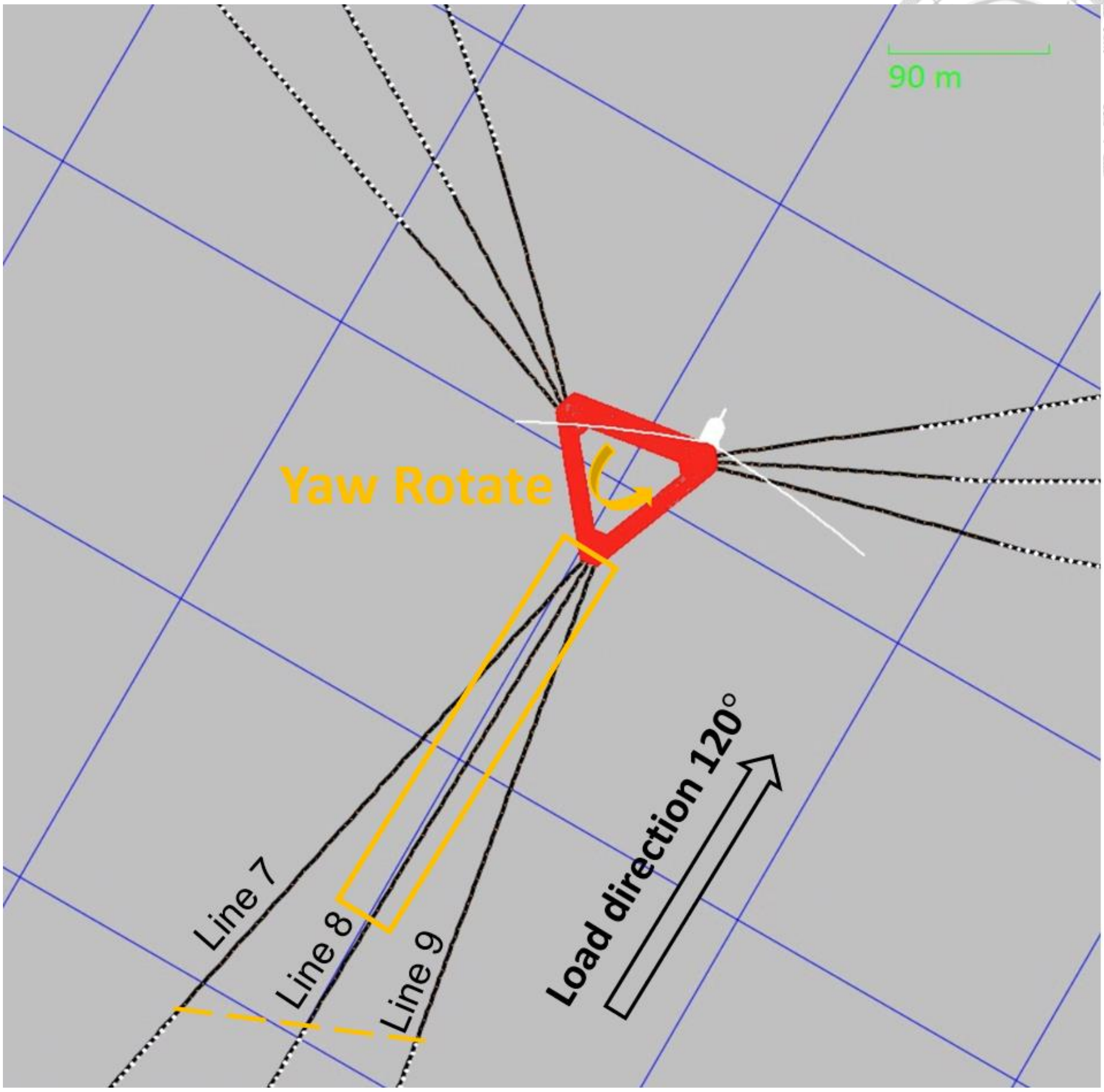

Figure 26: Static Simulation of TaidaFloat Off-Column Platform Mooring Line Response Under 120° Load Direction

In contrast, Figure 27 presents static simulation results for the VolturnUS center-column platform under a 120° load direction. Mooring line Line 8 aligns closely with the blue solid line indicating platform displacement along the load direction with minimal yaw rotation. The lack of significant yaw results in suspended segments of mooring lines Line 7, 8, and 9 having similar lengths ensuring evenly distributed loads within the

doi:10.6342/NTU202500993

mooring line cluster.

Figure 28 illustrates the relationship between environmental load directions and maximum mooring line tension for the VolturnUS center-column platform. The platform's symmetrical design yields consistent results for critical load directions at 0°, 120°, and 240°. This even load distribution lowers maximum tension significantly compared to the off-column design. Comparing maximum mooring line tension between the TaidaFloat off-column platform (Figure 25) and the VolturnUS center-column platform (Figure 28) reveals that at a 0° load direction where the main column aligns with the load both platforms exhibit similar maximum tension of approximately 10,000 kN on mooring lines Line 1, Line 2, and Line 3 due to negligible yaw rotation. However, when load directions change yaw rotation in the off-column platform creates significant mooring system design challenges. These findings highlight the critical role of platform symmetry in mitigating yaw-induced tension under multidirectional loads.

doi:10.6342/NTU202500993

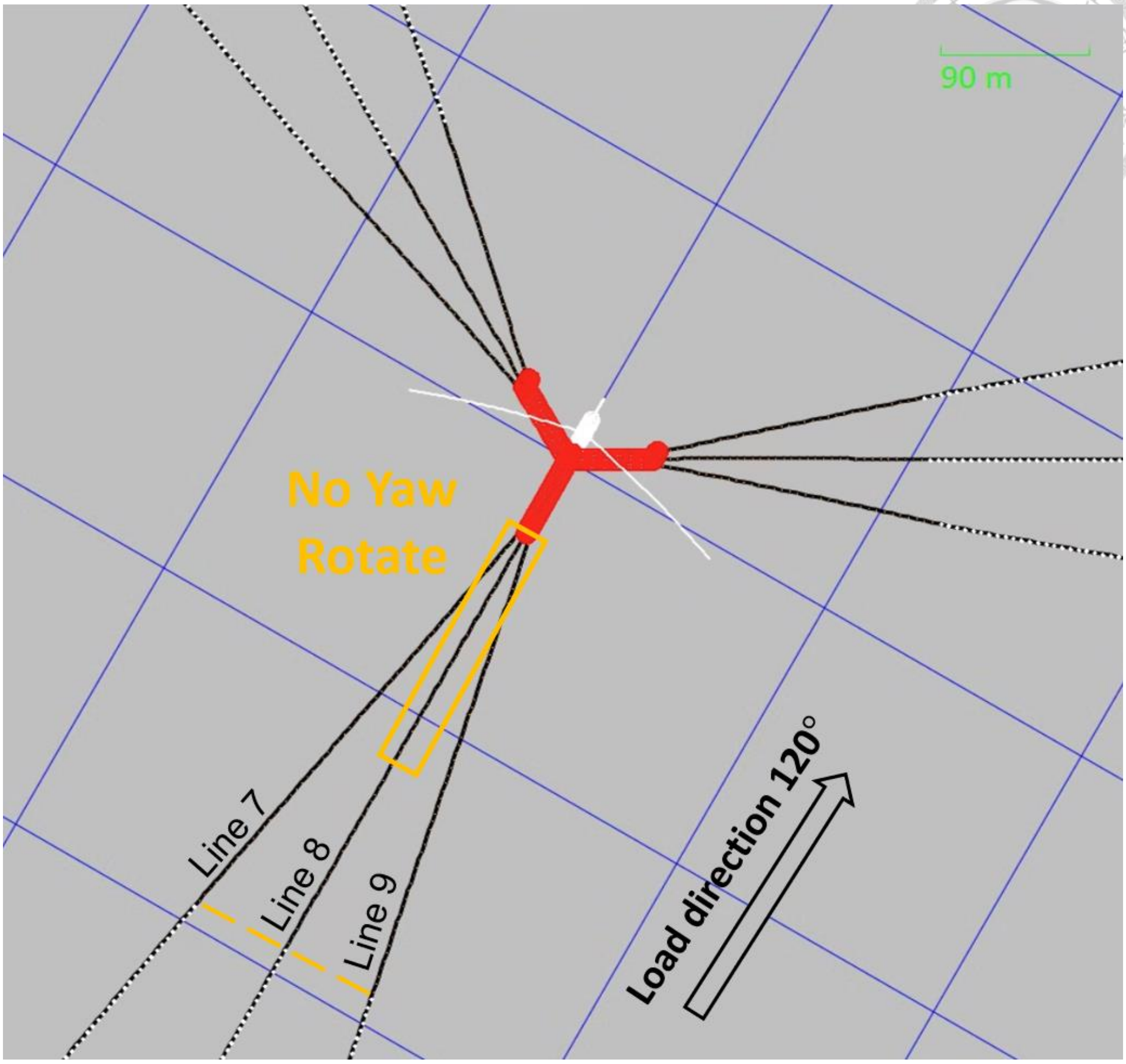

Figure 27: Static Simulation of VolturnUS Center-Column Platform Mooring Line Response Under 120° Load Direction

doi:10.6342/NTU202500993

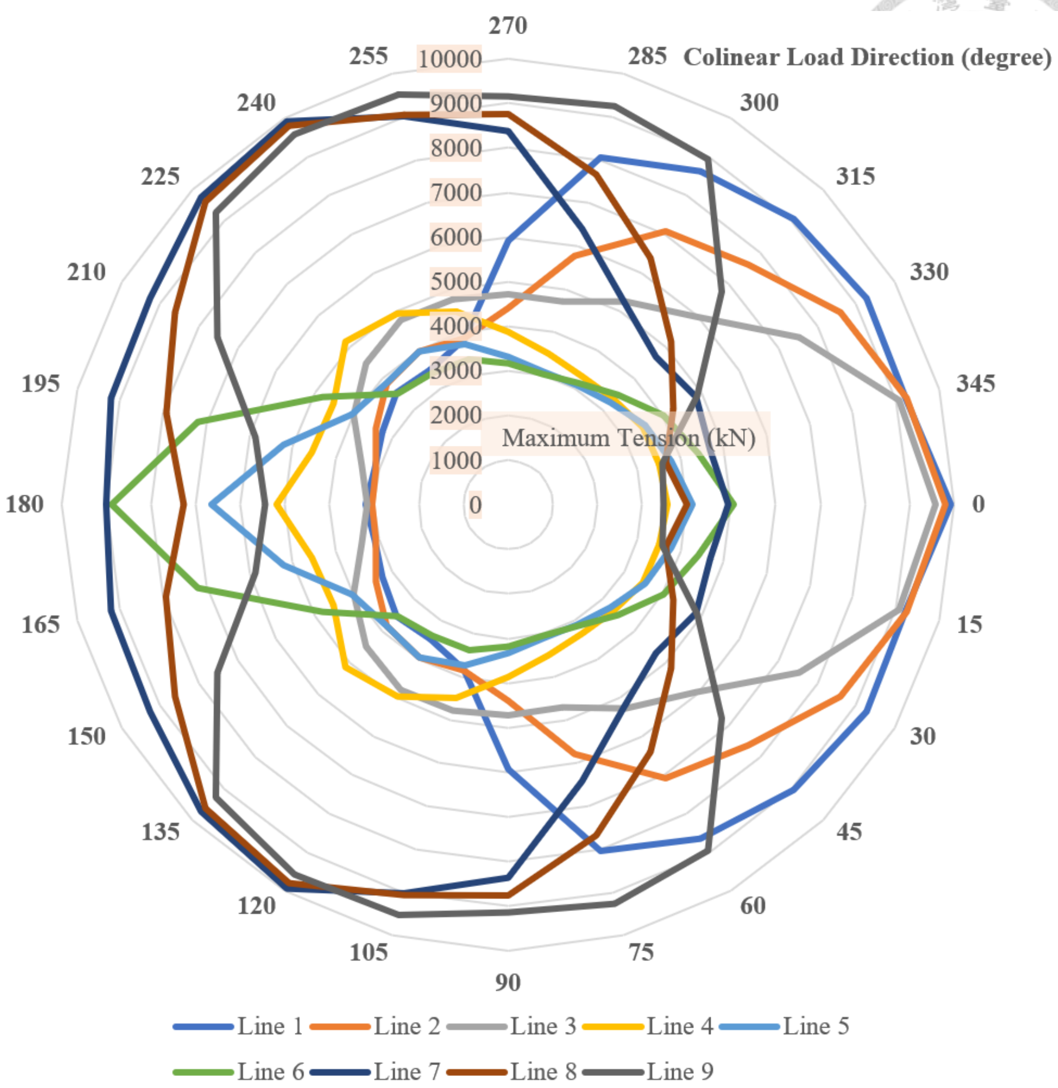

Figure 28: Maximum Mooring Line Tension vs. Environmental Load Directions for VolturnUS Center-Column Platform (Seed 111)

7.2.3 Critical Direction for Maximum Platform Offset

Figure 29 illustrates the relationship between environmental load directions and maximum platform offset. At 180°, mooring stiffness is minimized, resulting in the maximum platform offset. Thus, 180° is identified as the critical direction for offset.

doi:10.6342/NTU202500993

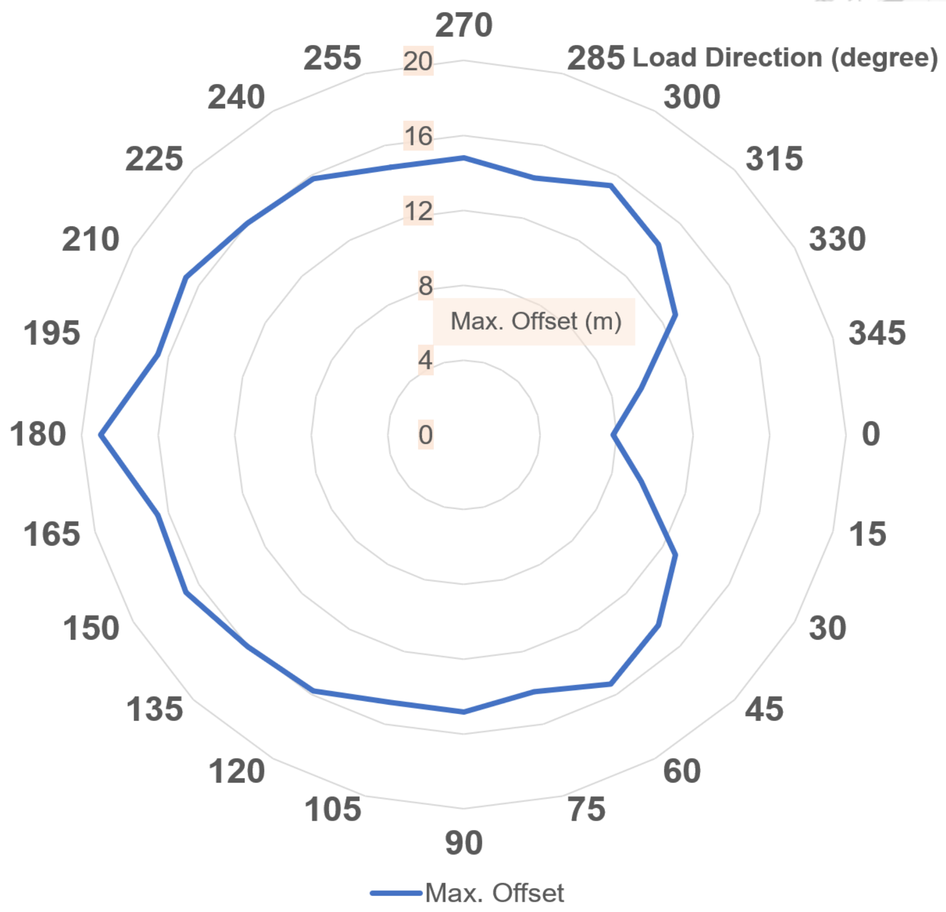

Figure 29: Maximum Platform Offset vs. Environmental Load Directions for Baseline All-Chain Mooring Design (Seed 111)

By focusing on the critical environmental load directions of 120° (maximum tension) and 180° (maximum offset), the design process for the all-chain mooring system was streamlined. Subsequent mooring analyses concentrate on these two critical directions.

7.3 Evaluation of Baseline All-Chain Mooring Design

Using the identified critical environmental load directions, the baseline all-chain mooring design was evaluated under DLC 6.1, with results summarized in Table 15. The maximum platform offset is 16.3 m, which complies with the design standard of 21 m.

doi:10.6342/NTU202500993

However, the maximum mooring tension is 16,911 kN, yielding a safety factor of 1.43, which falls below the required minimum of 1.67. Consequently, the design does not meet the maximum tension criteria, necessitating optimization to achieve full compliance with design standards.

Table 15: Evaluation Results of Baseline All-Chain Mooring Design under DLC 6.1

Criteria	Result Evaluation	Code Checks
Maximum Mooring Tension	16,911 kN (Line 7)	**Fail**
Safety Factor of Mooring Line	1.28<1.67	
Maximum Platform Offset	16.3 m (27% water depth)	**Pass**
Criteria of Platform Offset	16.3 m < 21 m	

7.4 Optimization of All-Chain Mooring Design

Building on the evaluation in Section 7.3, the baseline all-chain mooring configuration fails to meet the maximum tension design standard but demonstrates sufficient platform offset margin for optimization. Increasing the anchor radius and reducing pre-tension are expected to lower maximum mooring tension while maintaining offset within acceptable limits. Three pre-tension levels (5.7%, 6.6%, and 9.1% of Minimum Breaking Load, MBL) across seven anchor radii (840 m to 1,260 m, or 12 to 18 times the water depth) were investigated.

Figure 30 illustrates the maximum mooring line tension (multiplied by a safety factor

doi:10.6342/NTU202500993

of 1.67) for the 3x3 mooring configuration across varying anchor radii and pre-tension levels, compared against the MBL of a 160 mm chain (red line) as the design threshold. Cases exceeding this threshold fail to meet the maximum tension standard. The 9.1% MBL case (green dotted line) achieves compliance at an anchor radius of 1,260 m (18 times the water depth), the 6.6% MBL case (brown line with square markers) at 1,190 m (17 times the water depth), and the 5.7% MBL case (blue line with triangular markers) at 1,050 m (15 times the water depth). Lower pre-tension and larger anchor radii consistently reduce maximum tension, though offset constraints must be considered to ensure overall design feasibility.

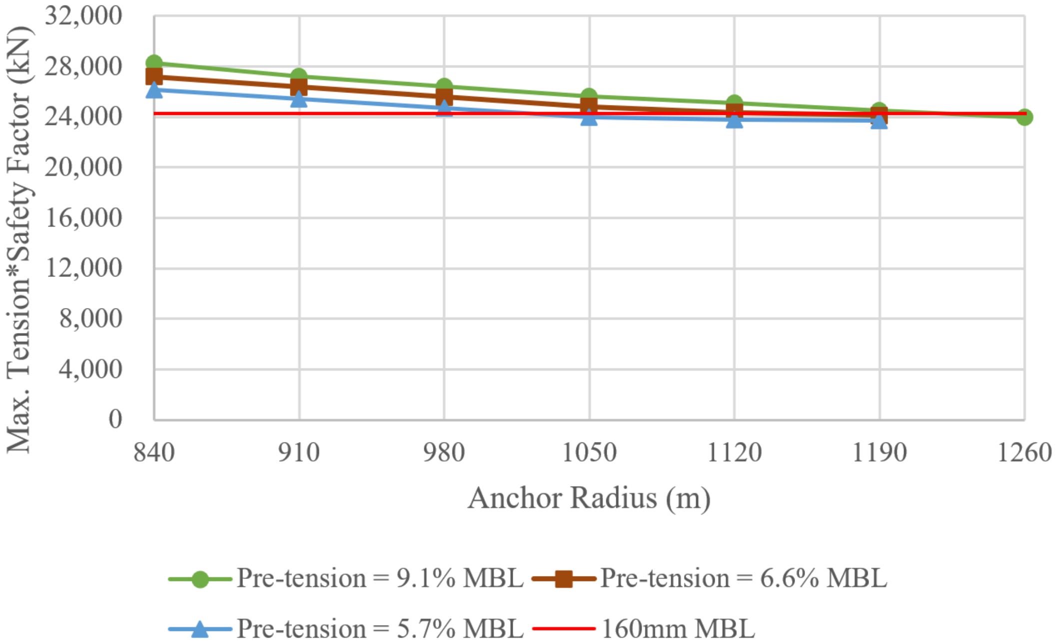

Figure 30: Maximum Mooring Tension vs. Anchor Radius for 3x3 All-Chain Mooring Configuration at Different Pre-Tension Levels

Notably, the maximum tension decreases nonlinearly with increasing anchor radius,

doi:10.6342/NTU202500993

with the rate of decrease slowing at larger radii. The tension values for the three pre-tension levels converge at higher radii (e.g., 1,260 m), indicating a marginal effect of further radius increases on tension reduction. This behavior stems from the Most Probable Maximum (MPM) method's sensitivity to extreme events driven by nonlinear effects, such as snap loads in low-stiffness catenary systems and second-order slow-drift motions. At smaller anchor radii, higher mooring stiffness amplifies floater motion responses, resulting in larger extreme tensions. As anchor radius increases, the mooring system's stiffness decreases significantly, approaching a minimum where further reductions have limited impact, and the response becomes dominated by catenary geometry. Since extreme wave conditions are consistent across all cases, the mooring system's load absorption capacity becomes similar at large radii, regardless of pre-tension, leading to convergence of MPM tensions.

To further understand this behavior, the mooring line tension spectra (Figure 31) were analyzed. For a given pre-tension level, smaller anchor radii produce higher spectral peaks due to increased mooring stiffness. Higher stiffness enhances sensitivity to environmental loads, amplifying dynamic tension variations and resulting in larger spectral peaks. Smaller radii also reduce system damping, further increasing the dynamic response to floater motions.

doi:10.6342/NTU202500993

The mooring line tension spectra exhibit consistent trends across anchor radii for each pre-tension level. For the 9.1% MBL case, the spectrum shows a single peak at approximately 0.08 Hz, corresponding to wave-frequency motions (first-order wave response). In contrast, the 6.6% and 5.7% MBL cases display an additional peak at approximately 0.04 Hz, reflecting low-frequency responses such as second-order slow-drift motions. This difference arises because higher pre-tension (9.1% MBL) increases mooring stiffness, raising the system's natural frequency and suppressing low-frequency responses, resulting in a single wave-frequency peak. Lower pre-tension (6.6% and 5.7% MBL) reduces stiffness, allowing the system to respond to low-frequency excitations, which manifest as the additional 0.04 Hz peak. These spectral characteristics account for the maximum tensions observed at smaller anchor radii, where increased stiffness enhances dynamic responses, and nonlinear effects such as snap loads and slow-drift motions dominate the extreme tension behavior

doi:10.6342/NTU202500993

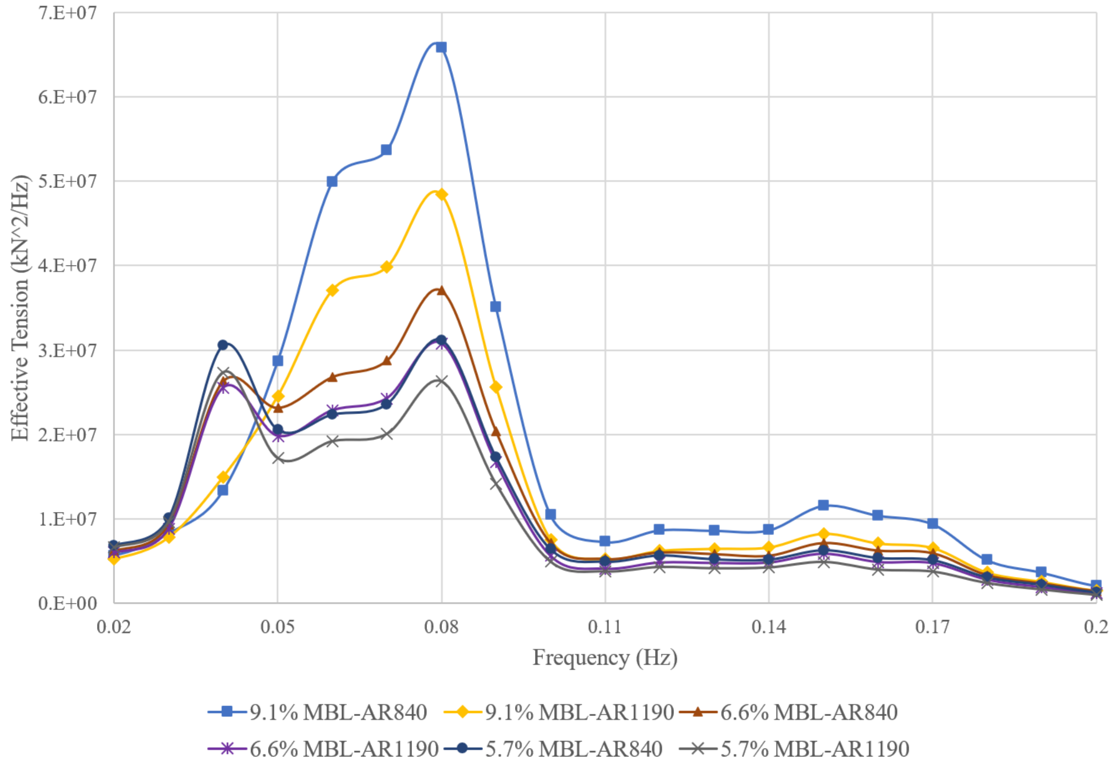

Figure 31: Mooring Line Tension Spectra for Various Pre-tension Levels and Anchor Radii

Figure 32 presents the maximum platform offset for the 3x3 mooring configuration across various anchor radii and pre-tension levels, with the red line indicating the offset limit of 30% of the water depth (21 m in this study). For the 5.7% MBL case (blue line with triangular markers), the offset exceeds the 21 m limit, reaching 21.2 m at a 980 m anchor radius (14 times the water depth) and 21.5 m at a 1,050 m radius (15 times the water depth). Table 16 summarizes the compliance of the 5.7% MBL case at a 1,050 m radius: the maximum tension of 14,371 kN (safety factor of 1.67) satisfies the design criteria, but the offset of 21.5 m exceeds the limit. This indicates that the 5.7% MBL pre-tension is insufficiently stiff, resulting in excessive platform displacement due to reduced

doi:10.6342/NTU202500993

mooring stiffness.

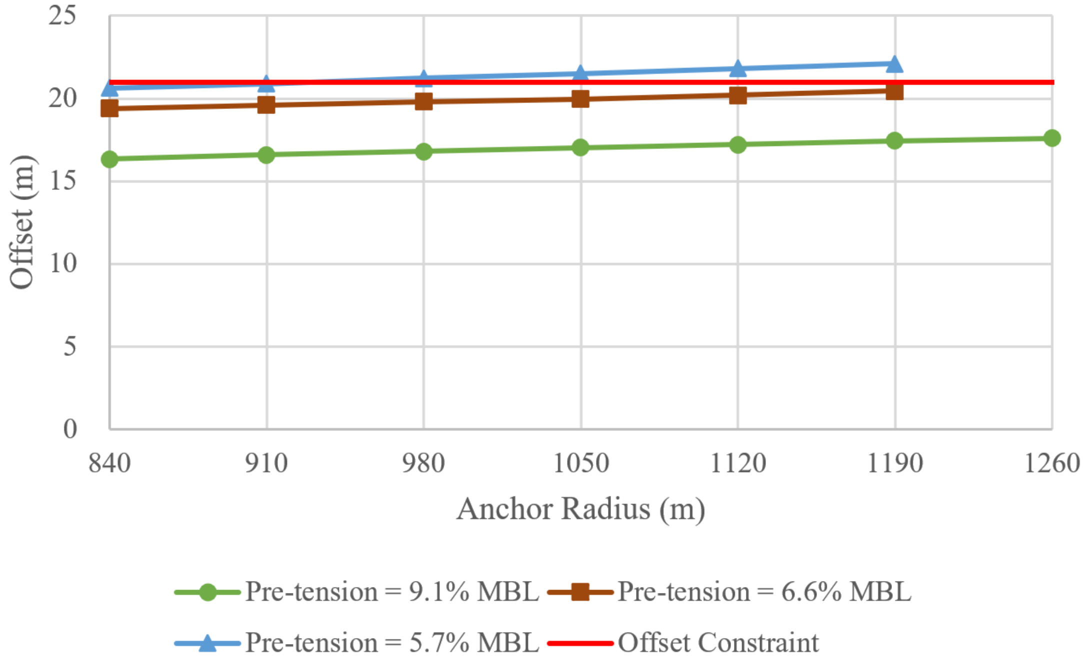

Figure 32: Maximum Platform Offset vs. Anchor Radius for 3x3 All-Chain Mooring Configuration at Different Pre-Tension Levels

Table 16: Summary of Mooring Design Results for 1,050 m Anchor Radius at 5.7% MBL Pre-Tension

Criteria	Result Evaluation	Code Checks
Maximum Mooring Tension	14,371 kN (Line 7)	**Pass**
Safety Factor of Mooring Line	1.69 > 1.67	
Maximum Platform Offset	21.5 m (31% water depth)	**Fail**
Criteria of Platform Offset	21.5 m > 21 m	

In contrast, the 9.1% MBL (green dotted line) and 6.6% MBL (brown line with square markers) cases remain below the 21 m offset threshold across all anchor radii,

doi:10.6342/NTU202500993

complying with offset standards. Table 17 details the 9.1% MBL case at a 1,260 m anchor radius: the maximum tension of 14,351 kN (safety factor of 1.67) meets the tension criteria, and the offset of 17.6 m is well below the 21 m limit. Similarly, Table 18 summarizes the 6.6% MBL case at a 1,190 m anchor radius: the maximum tension of 14,440 kN (safety factor of 1.67) satisfies the tension criteria, and the offset of 20.4 m complies with the limit. Thus, both pre-tension levels achieve compliant designs at anchor radii of 1,260 m (9.1% MBL) and 1,190 m (6.6% MBL), respectively.

Table 17: Summary of Mooring Design Results for 1,260 m Anchor Radius at 9.1% MBL Pre-Tension

<table>
<tr><th>Criteria</th><th>Result Evaluation</th><th>Code Checks</th></tr>
<tr><td>Maximum Mooring Tension</td><td>14,351 kN (Line 7)</td><td rowspan="2">Pass</td></tr>
<tr><td>Safety Factor of Mooring Line</td><td>1.69 > 1.67</td></tr>
<tr><td>Maximum Platform Offset</td><td>17.6 m (25% water depth)</td><td rowspan="2">Pass</td></tr>
<tr><td>Criteria of Platform Offset</td><td>17.6 m < 21 m</td></tr>
</table>

Table 18: Summary of Mooring Design Results for 1,190 m Anchor Radius at 6.6% MBL Pre-Tension

<table>
<tr><th>Criteria</th><th>Result Evaluation</th><th>Code Checks</th></tr>
<tr><td>Maximum Mooring Tension</td><td>14,440 kN (Line 7)</td><td rowspan="2">Pass</td></tr>
<tr><td>Safety Factor of Mooring Line</td><td>1.68 > 1.67</td></tr>
<tr><td>Maximum Platform Offset</td><td>20.4 m (29% water depth)</td><td rowspan="2">Pass</td></tr>
<tr><td>Criteria of Platform Offset</td><td>20.4 m < 21 m</td></tr>
</table>

doi:10.6342/NTU202500993

Reducing pre-tension from 9.1% to 6.6% MBL optimizes the all-chain mooring configuration by decreasing the required anchor radius from 1,260 m to 1,190 m, enhancing cost-efficiency through reduced material and installation demands. This aligns with the tension spectra findings (Figure 31), where lower pre-tension increases low-frequency responses (0.04 Hz peak), potentially contributing to larger offsets, but remains within limits for 6.6% MBL. Consequently, the 6.6% MBL pre-tension with a 1,190 m anchor radius is selected as the optimized all-chain mooring design, balancing tension compliance, offset constraints, and cost considerations.

doi:10.6342/NTU202500993

8 Clump-Weighted All-Chain Mooring Design

Following the optimization of the all-chain mooring configuration in Section 7.4, where a pre-tension of 6.6% of the MBL at a 1,190 m anchor radius was selected for its compliance with tension and offset standards, this section explores the integration of clump weights to further enhance the 3x3 mooring system. Section 7.4 revealed that a lower pre-tension of 5.7% MBL at a 1,050 m anchor radius satisfied maximum tension requirements but exceeded the 21 m offset limit due to insufficient stiffness, while a higher pre-tension of 6.6% MBL resolved the offset issue at the cost of a larger anchor radius. To enable lower pre-tensions (e.g., 5.7% or 4.4% MBL) while meeting offset constraints, clump weights are introduced to increase mooring stiffness by enhancing vertical loads and modifying the catenary geometry, thereby improving restoring forces and reducing platform offset.

The section is structured as follows: Section 8.1 describes the 8-tonne clump weight design adopted in this study. Section 8.2 evaluates the response of the clump-weighted mooring system to critical environmental load directions, including wave, wind, and current combinations. Section 8.3 analyzes the effect of varying the starting point of clump weights along the mooring line on tension and offset. Section 8.4 optimizes the clump-weighted configuration by adjusting the number of clump weights per line to

doi:10.6342/NTU202500993

minimize maximum tension and offset while ensuring cost-efficiency, selecting the optimal design that complies with tension and offset standards.

8.1 Clump Weight Design

Preliminary research by Yuki [40] demonstrated that 13 units of 3-tonne clump weights had limited effect on reducing the offset of TaidaFloat platform. This study adopts an enhanced design with 8-tonne clump weights per mooring line to increase vertical load and modify catenary geometry. These changes improve mooring stiffness and restoring forces. The detailed parameters of the clump weight design are provided in Table 19, with the geometry illustrated in Figure 33.

Table 19: Parameters of 8-Tonne Clump Weights for TaidaFloat Mooring Design

Mass	8 tones
Volume	1.02 m^3
Length	1.97 m
Outer Diameter	0.97 m
Inner Diameter	0.6 m
Chain Diameter	0.17 m
Drag Area (x; y; z)	0.74 m^2; 1.71 m^2; 1.71 m^2
Drag Coefficient (x; y; z)	0.7; 0.6; 0.6

doi:10.6342/NTU202500993

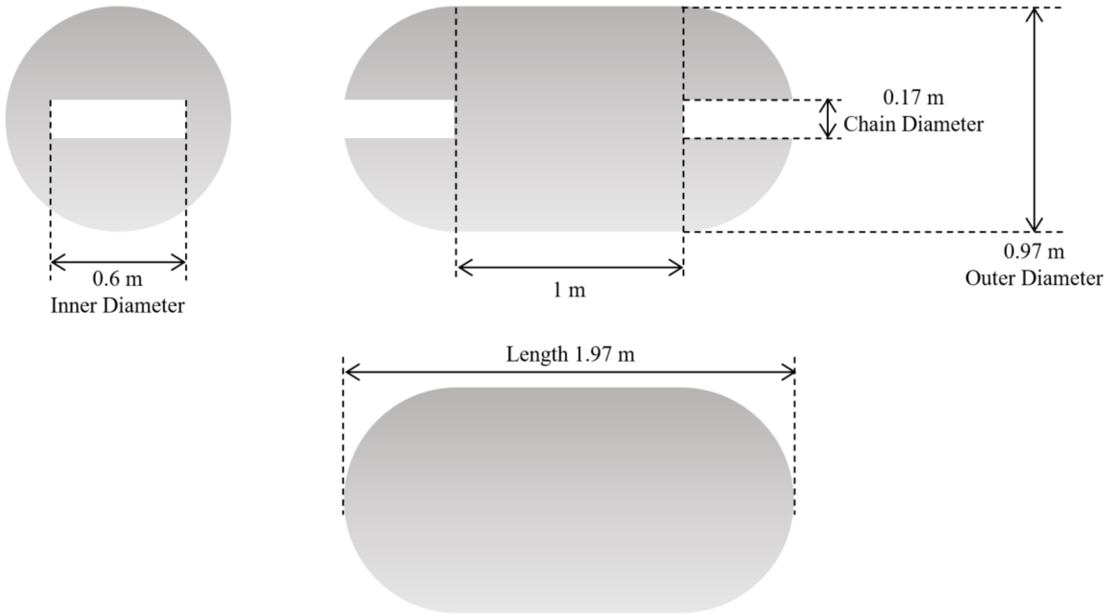

Figure 33: Geometry of 8-Tonne Clump Weight Configuration

8.2 Critical Environmental Load Directions for Clump-Weighted Mooring Design

Section 7.2.1 showed that for the 3x3 all-chain mooring system without clump weights, the critical directions for maximum mooring tension are 120° and 240°. The critical direction for maximum offset is 180°. Clump weights increase mooring stiffness and alter FOWT motion. This necessitates a reassessment of critical environmental load directions.

This analysis employs an initial pre-tension of 4.4% MBL at a 980 m anchor radius. Eleven 8-tonne clump weights are spaced 5 m apart, starting 100 m from the fairlead. This increases the effective pre-tension to 5.9% MBL due to added vertical load. Table

doi:10.6342/NTU202500993

20 summarizes the configuration. Given consistent trends across multiple random wave seeds, results are reported for seed 111 to streamline the analysis. Figure 34 illustrates the relationship between environmental load directions and maximum mooring line tension. The critical tension directions shift to 150° and 210° compared to 120° and 240° in the all-chain configuration without clump weights due to altered mooring dynamics.

The maximum platform offset, defined in Section 7.2.2, is analyzed in Figure 35, which depicts its variation with environmental load directions. The critical direction for maximum offset remains 180°, consistent with the all-chain configuration without clump weights. By identifying 150° for tension and 180° for offset as the critical directions, subsequent analyses can focus on these cases, simplifying the design process and reducing computational effort for the clump-weighted all-chain mooring configuration.

Table 20: Mooring Configuration for Critical Environmental Load Direction Analysis with Clump Weights

Mooring Type	All chain (studless)
Mooring Pattern	3x3 (Three lines on each column)
Anchor Radius	980 m (14 times water depth)
Mooring Line Length	940 m
Corrosion Allowance	0.4 mm per year
Chain Diameter (new)	170 mm
Chain Diameter (end of life)	160 mm
Chain Grade	R4S
Minimum Breaking Load (new)	26,708 kN
Minimum Breaking Load (end of life)	24,281 kN
Pre-tension	1,567 kN (5.9% MBL)
In Air Weight (new)	504 kg/m

doi:10.6342/NTU202500993

In Water Weight (new)	575 kg/m
Axial Stiffness of Chain (new)	2.468e6 kN
Drag Coefficients (Normal, Tangential)	2.4, 1.15
Added Mass Coefficients (Normal, Tangential)	2.0, 1.0
Clump Weights Number	11 units per line, Only on Line 4 ~ Line9
Clump Weights Starting Point	80 m from the fairlead
Clump Weights Spacing	5 m

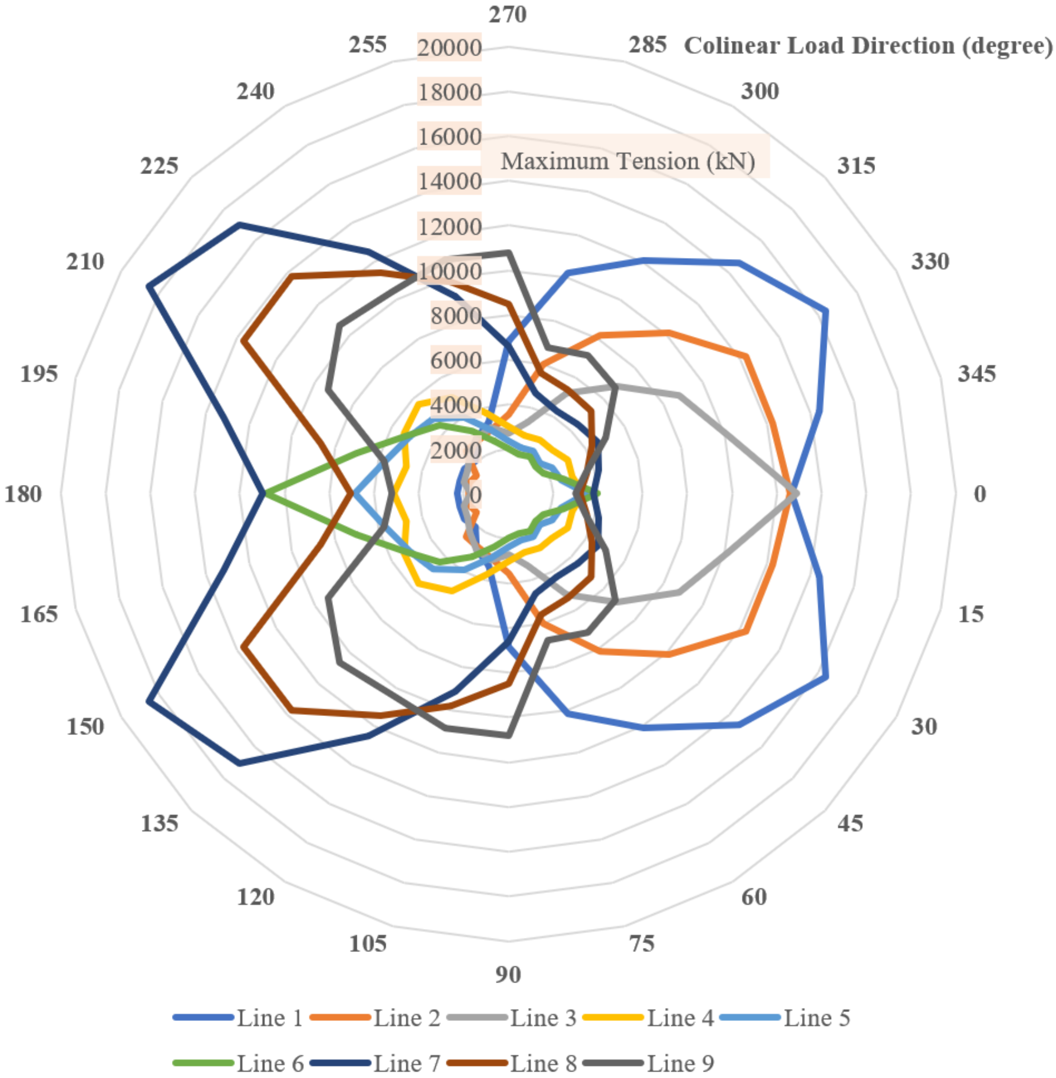

Figure 34: Maximum Mooring Line Tension vs. Environmental Load Directions for Clump-Weighted Mooring Design (Seed 111)

doi:10.6342/NTU202500993

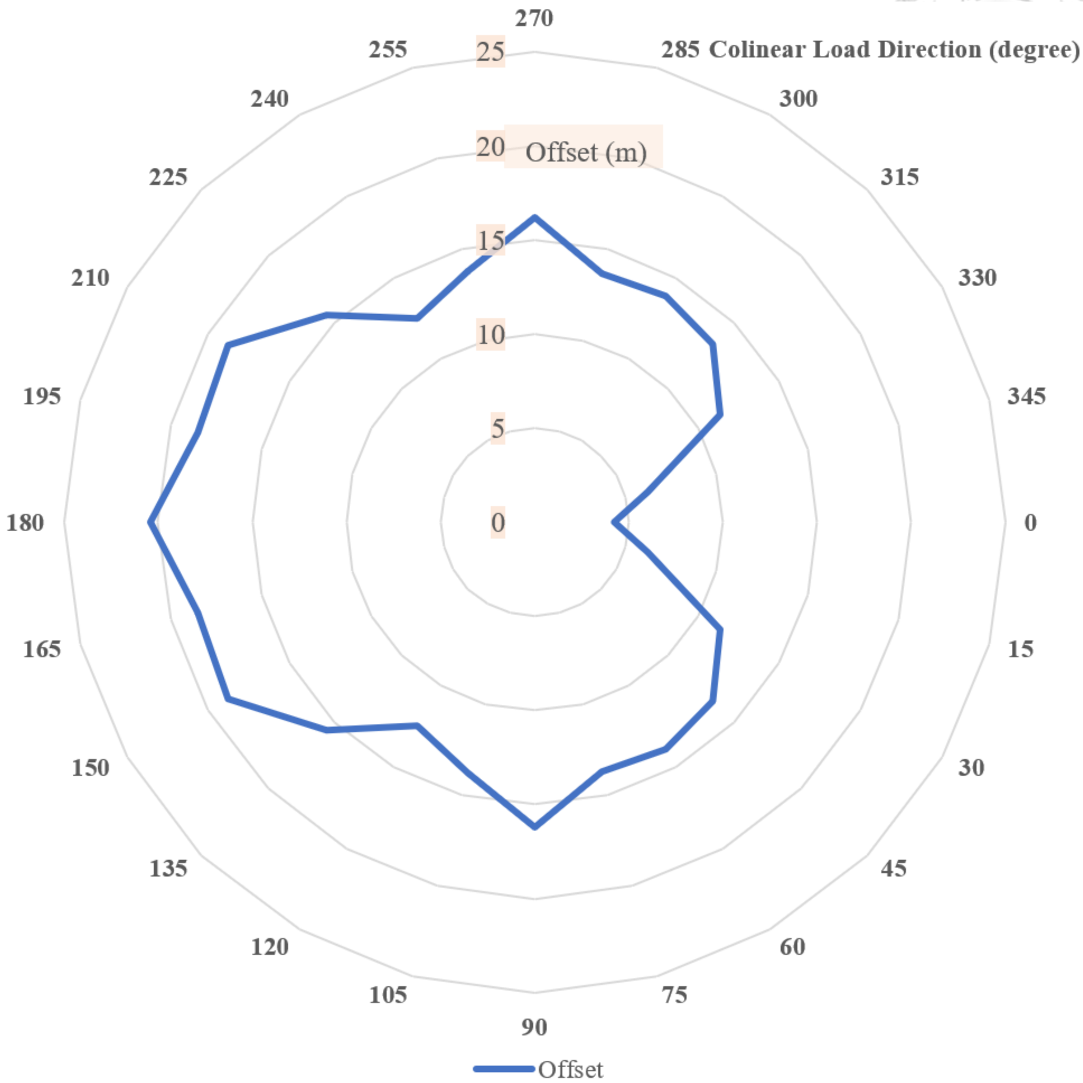

Figure 35: Maximum Platform Offset vs. Environmental Load Directions for Clump-Weighted Mooring Design (Seed 111)

8.3 Analysis of Clump Weight Starting Point on Mooring Performance

This subsection investigates the effect of varying the starting point of 8-tonne clump weights on the performance of the all-chain mooring system across three anchor radii: 980 m, 910 m, and 840 m. It analyzes the impact of 11 clump weights on maximum tension and platform offset to optimize the mooring profile for reduced anchor radius and

doi:10.6342/NTU202500993

compliance with design standards.

Four starting points (80 m, 100 m, 120 m, 150 m from the fairlead) with 5 m spacing between clump weights are tested. These points alter the mooring profile's catenary shape and vertical load distribution, which affect effective pre-tension. The mooring profiles use the 80 m starting point as a reference for visualization, as shown in Figure 36. Table 21–Table 23 detail the configurations and pre-tension values for each starting point and anchor radius.

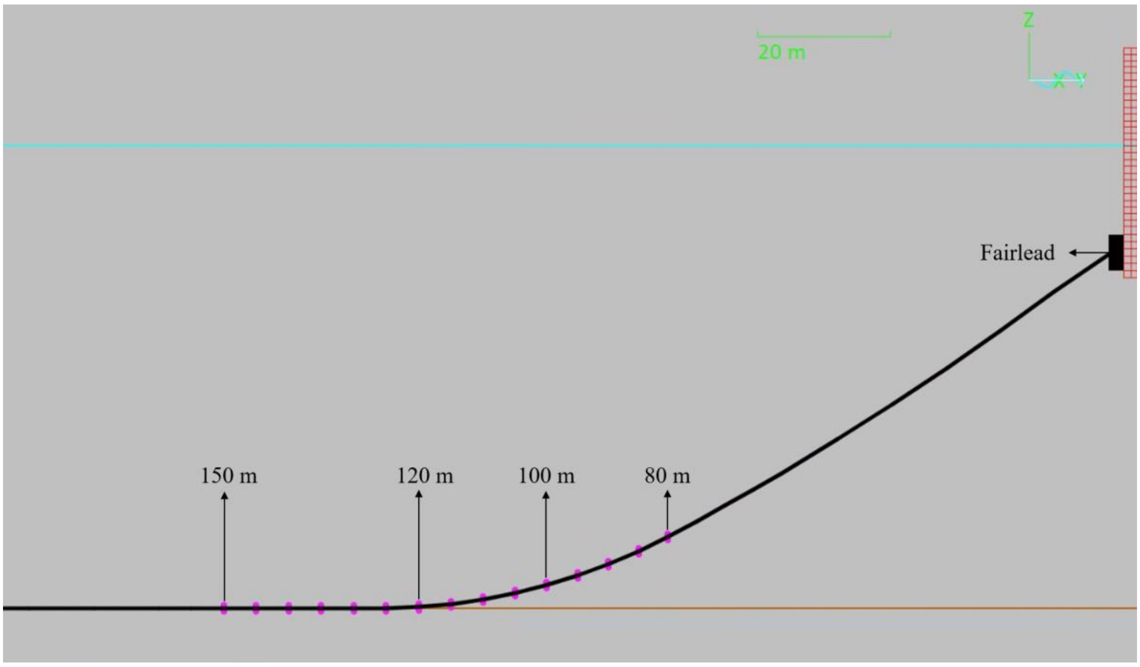

Figure 36: Clump Weight Starting Point Points on Mooring Lines with 80 m Fairlead Profile

doi:10.6342/NTU202500993

Table 21: Mooring Configuration for Clump Weight Starting Points at 980 m Anchor Radius

Mooring Type	All Chain with Clump Weights			
Mooring Pattern	3x3 (Three lines on each column)			
Anchor Radius	980 m			
Mooring Line Length	940 m			
Pre-tension	1,185 kN (4.4% MBL)	1,326 kN (5% MBL)	1,567 kN (5.9% MBL)	1,872 kN (7% MBL)
No. of Clump Weights per Line (Only Lines 4–9)	11 units			
Clump Weights Starting Point (From the fairlead)	150 m	120 m	100 m	80 m
Clump Weights Spacing	5 m			

Table 22: Mooring Configuration for Clump Weight Starting Points at 910 m Anchor Radius

Mooring Type	All Chain with Clump Weights			
Mooring Pattern	3x3 (Three lines on each column)			
Anchor Radius	910 m			
Mooring Line Length	870 m			
Pre-tension	1,185 kN (4.4% MBL)	1,326 kN (5% MBL)	1,567 kN (5.9% MBL)	1,872 kN (7% MBL)
No. of Clump Weights per Line (Only Lines 4–9)	11 units			
Clump Weights Starting Point (From the fairlead)	150 m	120 m	100 m	80 m
Clump Weights Spacing	5 m			

doi:10.6342/NTU202500993

Table 23: Mooring Configuration for Clump Weight Starting Points at 840 m Anchor Radius

Mooring Type	All Chain with Clump Weights			
Mooring Pattern	3x3 (Three lines on each column)			
Anchor Radius	840 m			
Mooring Line Length	800 m			
Pre-tension	1,185 kN (4.4% MBL)	1,326 kN (5% MBL)	1,567 kN (5.9% MBL)	1,872 kN (7% MBL)
No. of Clump Weights per Line (Only Lines 4–9)	11 units			
Clump Weights Starting Point (From the fairlead)	150 m	120 m	100 m	80 m
Clump Weights Spacing	5 m			

Table 24–Table 26 present the maximum tension and offset results. At the 980 m anchor radius, the 80 m and 100 m starting points meet tension and offset standards. At 910 m, only the 100 m point complies. At 840 m, none of the points satisfy the standards. These results show that 11 clump weights reduce the anchor radius from 1,190 m in Section 7.4 to 910 m, improving economic viability.

All anchor radii exhibit consistent trends. The 100 m starting point yields the lowest maximum tension. Tensions are slightly higher at 80 m and 120 m, and significantly higher at 150 m. For offset, the 80 m and 100 m points produce the lowest values. Offsets increase at 120 m and 150 m. The 100 m point optimizes tension and offset by balancing vertical load distribution and minimizing dynamic responses. This aligns with Li et al. [16], who found similar optimal placements for a center-column semi-submersible FOWT

doi:10.6342/NTU202500993

under typhoon conditions.

A starting point of 100 m from the fairlead is recommended as the baseline for further clump weight analyses in this study. It supports the goal of optimizing the mooring design for a smaller anchor radius and improved cost-efficiency.

Table 24: Maximum Tension and Offset Results for Clump Weight Starting Points at 980 m Anchor Radius

Clump Weights Starting Point (From the fairlead)	150 m	120 m	100 m	80 m
Maximum Mooring Tension	15,761 kN	14,592 kN	13,651 kN	14,116 kN
Safety Factor of Mooring Line	1.54 < 1.67	1.66 < 1.67	1.78 > 1.67	1.72 > 1.67
Tension Criteria Code Check	**Fail**	**Fail**	**Pass**	**Pass**
Maximum Platform Offset	21.9m < 21m	21.3m < 21m	21m = 21m	21m = 21m
Offset Criteria Code Check	**Fail**	**Fail**	**Pass**	**Pass**

Table 25: Maximum Tension and Offset Results for Clump Weight Starting Points at 910 m Anchor Radius

Clump Weights Starting Point (From the fairlead)	150 m	120 m	100 m	80 m
Maximum Mooring Tension	16,239 kN	14,989 kN	14,050 kN	14,609 kN
Safety Factor of Mooring Line	1.50 < 1.67	1.62 < 1.67	1.73 > 1.67	1.66 < 1.67
Tension Criteria Code Check	**Fail**	**Fail**	**Pass**	**Fail**
Maximum Platform Offset	21.6m < 21m	21m = 21m	20.8m < 21m	20.8m < 21m
Offset Criteria Code Check	**Fail**	**Pass**	**Pass**	**Pass**

doi:10.6342/NTU202500993

Table 26: Maximum Tension and Offset Results for Clump Weight Starting Points at 840 m Anchor Radius

Clump Weights Starting Point (From the fairlead)	150 m	120 m	100 m	80 m
Maximum Mooring Tension	17,300 kN	15,177 kN	14,766 kN	15,171 kN
Safety Factor of Mooring Line	1.40 < 1.67	1.60 < 1.67	1.64 < 1.67	1.60 < 1.67
Tension Criteria Code Check	**Fail**	**Fail**	**Fail**	**Fail**
Maximum Platform Offset	21.4m > 21m	20.8m < 21m	20.6m < 21m	20.6m < 21m
Offset Criteria Code Check	**Fail**	**Pass**	**Pass**	**Pass**

8.4 Optimization of Clump Weight Numbers per Mooring Line

This subsection optimizes the clump-weighted mooring system by evaluating the performance of different numbers of clump weights per mooring line. It builds on Section 8.3's finding that a 100 m starting point is optimal. The analysis focuses on two anchor radii: 910 m, which met tension and offset standards with 11 clump weights per line, and 840 m, which did not comply with 11 clump weights. For the 910 m case, the study assesses whether reducing to 10 clump weights maintains compliance while lowering material and installation costs. For the 840 m case, it examines whether increasing to 12 clump weights achieves compliance to further reduce the anchor radius. Table 27 details the configurations, and Table 28 summarizes the results.

For the 910 m anchor radius, reducing to 10 clump weights increases maximum

doi:10.6342/NTU202500993

tension and offset beyond the design standards. This confirms that 11 clump weights per line is optimal for the 910 m radius, balancing performance and efficiency. For the 840 m anchor radius, increasing to 12 clump weights lowers maximum tension to meet the design standard, while the already compliant offset decreases further. This enables the 840 m radius to satisfy both tension and offset standards, significantly reducing the anchor radius from 1,190 m in Section 7.4.

Varying the number of clump weights affects mooring stiffness and catenary geometry, which influence dynamic responses. Fewer clump weights at 910 m reduce stiffness, increasing floater motions and thus tension and offset. Adding a clump weight at 840 m enhances stiffness, mitigating extreme tensions.

The configuration with 12 clump weights per line at an 840 m anchor radius and a 100 m starting point is selected as the final optimized clump-weighted mooring design. This design reduces the anchor radius by 29% compared to the 1,190 m all-chain design in Section 7.4, improving economic viability through lower material and installation costs. It demonstrates the effectiveness of clump weights in enabling smaller anchor radii while meeting all design standards.

doi:10.6342/NTU202500993

Table 27: Configurations for Varying Numbers of Clump Weights per Mooring Line at 910 m and 840 m Anchor Radii

Mooring Type	All Chain with Clump Weights			
Mooring Pattern	3x3 (Three lines on each column)			
Anchor Radius	910 m		840 m	
Mooring Line Length	870 m		800 m	
Pre-tension	1,567 kN (5.9% MBL)			
No. of Clump Weights per Line (Only Lines 4–9)	11 units	10 units	12 units	11 units
Clump Weights Starting Point	100 m from the fairlead			
Clump Weights Spacing	5 m			

Table 28: Maximum Tension and Offset Results for Varying Numbers of Clump Weights per Mooring Line at 910 m and 840 m Anchor Radii

Anchor Radius	910 m		840 m	
Mooring Line Length	870 m		800 m	
No. of Clump Weights per Line (Only Lines 4–9)	11 units	10 units	12 units	11 units
Maximum Mooring Tension	14,050 kN	14,613 kN	14,067 kN	14,766 kN
Safety Factor of Mooring Line	1.73 > 1.67	1.66 > 1.67	1.73 < 1.67	1.64 < 1.67
Tension Criteria Code Check	**Pass**	**Fail**	**Pass**	**Fail**
Maximum Platform Offset	20.8m < 21m	21.1m > 21m	20.3 < 21 m	20.6m < 21m
Offset Criteria Code Check	**Pass**	**Fail**	**Pass**	**Pass**

9 Conclusions

This delivers a comprehensive analysis of the TaidaFloat, a 15 MW off-column semi-submersible FOWT, focusing on platform stability, hydrodynamic performance, and mooring system design. By addressing the scarcity of open-source data on off-column

doi:10.6342/NTU202500993

semi-submersible designs, this study provides a critical reference for global offshore wind research. It consolidates two years of the author's master's research, integrating a conference paper, an industrial report, a technical specification, and an unpublished journal manuscript in Appendix A.

The thesis presents five key findings:

1. Yaw Rotation from Off-column Design: The off-column semi-submersible's asymmetrical geometry generates a yaw moment from wind thrust on the turbine when the wind is misaligned with the main column bearing the turbine, inducing platform yaw rotation. This leads to uneven load distribution within the mooring line cluster, with one line experiencing excessively high tension. Aligning the main column with the wind mitigates yaw in unidirectional wind conditions. However, in the Taiwan Strait's multidirectional typhoon environment, extreme loads from varying directions trigger yaw rotation and tension concentration, presenting significant mooring design challenges. Conversely, center-column semi-submersibles, with their symmetrical design and centrally positioned turbine, achieve balanced load distribution and lower mooring tensions.

2. Large Mooring Footprint in Taiwan Strait: The Taiwan Strait's extreme typhoon conditions and intermediate water depths demand a large mooring footprint. An all-chain

doi:10.6342/NTU202500993

3×3 mooring system without clump weights requires a 1,190 m anchor radius to meet tension and offset regulations (Section 7.4). This expansive footprint reduces wind farm area efficiency and escalates costs due to the need for nine long mooring chains. These conditions underscore the necessity for innovative FOWT solutions tailored to the region's unique environmental challenges.

3. Clump Weights for Tension Reduction: Clump weights significantly reduce maximum mooring tension and offset in the Taiwan Strait's typhoon conditions and intermediate water depths, making them a highly effective method for minimizing anchor radius. The optimized clump-weighted all-chain mooring design employs 12 clump weights per line across six lines in two side column clusters, achieving an 840 m anchor radius. This represents a 29% reduction compared to the 1190 m all-chain design without clump weights. The smaller footprint reduces material and installation costs, improving economic viability.

4. Current Load Impact in Dynamic Simulation: This study incorporates the drag coefficient into the FOWT dynamic simulation, comprehensively modeling the coupled effects of wind, waves, and currents to replicate real-world environmental conditions. Unlike many academic FOWT studies that omit current loads, this analysis reveals their significant impact on maximum mooring tension. While the thesis prioritizes mooring

doi:10.6342/NTU202500993

design and does not deeply explore current effects, preliminary results indicate that neglecting current forces severely underestimates environmental loads on the mooring system. Future research on mooring tension should include current forces to ensure accurate load assessments.

5. Efficient Mooring Tension Calculation: A Python script developed in this thesis employs the Most Probable Maximum (MPM) method to calculate maximum mooring tension, yielding results 5 to 10% lower than the mean of all seeds in Appendix A.2. This aligns with DNV regulations, which consider the mean of all seeds overly conservative, and supports industry practices favoring less conservative designs. The MPM method facilitates rational mooring designs, reducing anchor radii and system costs.

Despite these advancements, the optimized mooring system, with an 840 m anchor radius, nine 800 m mooring lines and 72 8-tonne clump weights, remains costly and complex to install. A preliminary chain-polyester-chain mooring study in Appendix A.2 reveals limited benefits in the Taiwan Strait's intermediate water depths, as polyester rope's seabed contact restrictions limit its feasible section to 50 m, offering negligible tension reduction. These findings underscore the inherent limitations of off-column semi-submersible mooring systems, which demand large anchor radii and substantial steel materials.

doi:10.6342/NTU202500993

Reference

1. Agreement, P. *Paris agreement*. in *report of the conference of the parties to the United Nations framework convention on climate change (21st session, 2015: Paris). Retrived December*. 2015. HeinOnline.
2. IEA, I., *Net zero roadmap: A global pathway to keep the 1.5 C goal in reach.* International Energy Agency Report, 2023.
3. Barthelmie, R.J., *A brief review of offshore wind energy activity in the 1990's.* Wind Engineering, 1998: p. 265-273.
4. Larsson, A.-K., *The environmental impact from an offshore plant.* Wind Engineering, 1994: p. 213-218.
5. Nielsen, F.G., T.D. Hanson, and B.r. Skaare. *Integrated dynamic analysis of floating offshore wind turbines*. in *International conference on offshore mechanics and arctic engineering*. 2006.
6. Shafiee, M., *Failure analysis of spar buoy floating offshore wind turbine systems.* Innovative Infrastructure Solutions, 2023. **8**(1): p. 28.
7. Ma, K.-T., et al., *Mooring system engineering for offshore structures*. 2019: Gulf Professional Publishing.
8. Li, Y., et al., *Analysis on restoring stiffness and its hysteresis behavior of slender catenary mooring-line.* Ocean Engineering, 2020. **209**: p. 107521.
9. Ma, K.-T., et al., *Review of Anchor Solutions for Floating Offshore Wind Turbines.*
10. Brommundt, M., et al., *Mooring system optimization for floating wind turbines using frequency domain analysis.* Energy Procedia, 2012. **24**: p. 289-296.
11. Benassai, G., et al., *Mooring control of semi-submersible structures for wind turbines.* Procedia Engineering, 2014. **70**: p. 132-141.
12. Campanile, A., V. Piscopo, and A. Scamardella, *Mooring design and selection for floating offshore wind turbines on intermediate and deep water depths.* Ocean Engineering, 2018. **148**: p. 349-360.
13. Hordvik, T., *Design analysis and optimisation of mooring system for floating wind turbines*. 2011, Norges teknisk-naturvitenskapelige universitet, Fakultet for ….
14. Pan, Q., M.Y. Mahfouz, and F. Lemmer. *Assessment of mooring configurations for the IEA 15MW floating offshore wind turbine*. in *Journal of Physics: Conference Series*. 2021. IOP Publishing.

doi:10.6342/NTU202500993

15. Xu, K., *Design and analysis of mooring system for semi-submersible floating wind turbine in shallow water.* 2020.

16. Li, J., et al., *Study on the mooring systems attaching clump weights and heavy chains for improving the typhoon resistance of floating offshore wind turbines.* Ocean Engineering, 2024. **311**: p. 118734.

17. Robertson, A., et al., *Definition of the semisubmersible floating system for phase II of OC4*. 2014, National Renewable Energy Lab.(NREL), Golden, CO (United States).

18. Allen, C., et al., *Definition of the UMaine VolturnUS-S reference platform developed for the IEA wind 15-megawatt offshore reference wind turbine*. 2020, National Renewable Energy Lab.(NREL), Golden, CO (United States); Univ. of ….

19. Offshorewind.biz, *ASM Industries Adds WindFloat Atlantic to Its Checklist*. 2018.

20. Gaertner, E., et al., *Definition of the IEA 15-megawatt offshore reference wind turbine.* 2020.

21. ABS, *Guide for Building and Classing Floating Offshore Wind Turbines.* 2020.

22. DNV, *Offshore Standards: Position mooring. DNV-OS-E301.* 2018.

23. Jan, S., et al., *Seasonal variation of the circulation in the Taiwan Strait.* Journal of Marine Systems, 2002. **35**(3-4): p. 249-268.

24. 4COffshore. *Global Offshore Wind Farms Database*. 2014; Available from: https://map.4coffshore.com/offshorewind/https://map.4coffshore.com/offshorewind/.

25. Chen, C.-A., et al. *Design of Mooring System for a 15MW Semi-Submersible, TaidaFloat, in Taiwan Strait*. in *International Conference on Offshore Mechanics and Arctic Engineering*. 2023. American Society of Mechanical Engineers.

26. *Central Weather Administration, Taiwan (ROC)*. Available from: https://www.cwa.gov.tw/V8/C/.

27. *National Oceanic and Atmospheric Administration, Department of Commerce, U.S.* . Available from: https://www.noaa.gov/.

28. Commission, I.I.E., *IEC 61400-1: 2019: Wind energy generation systems-Part 1: Design requirements*. 2019, IEC.

29. ABS, *Guide for Position Mooring Systems.* 2018.

30. Shu, H., et al. *API RP 2SK 4th edition-an updated stationkeeping standard for the*

doi:10.6342/NTU202500993

global offshore environment. in *Offshore Technology Conference*. 2018. OTC.

31. Veritas, B., *Classification of mooring systems for permanent offshore units.* Guidance Note NI, 2012. **493**.

32. Guo, C., et al., *Seasonal responses of nutrient to hydrology and biology in the southern Yellow Sea.* Continental Shelf Research, 2020. **206**: p. 104207.

33. Ivanov, G., I.-J. Hsu, and K.-T. Ma, *Design considerations on Semi-Submersible columns, bracings and pontoons for floating wind.* Journal of Marine Science and Engineering, 2023. **11**(9): p. 1663.

34. Hsu, I.-J., et al. *Optimization of Semi-Submersible hull design for floating offshore wind turbines*. in *International Conference on Offshore Mechanics and Arctic Engineering*. 2022. American Society of Mechanical Engineers.

35. Wu, K., et al. *Technology Development of a Floating Offshore Wind Turbine," TaidaFloat*. in *Taiwan Wind Energy Conference*. 2023.

36. Edwards, E.C., et al., *Evolution of floating offshore wind platforms: A review of at-sea devices.* Renewable and Sustainable Energy Reviews, 2023. **183**: p. 113416.

37. DNV, *Floating wind turbine structures. DNV-ST-0119.* 2021.

38. NTU, *TaidaFloat Mooring Analysis Report.* Approval in Principle, American Bureau of Shipping, 2023.

39. Chen, M., et al., *Study on mooring design of 15 MW floating wind turbines in South China Sea.* Journal of marine science and engineering, 2023. **12**(1): p. 33.

40. Yuki, I., *Influence of Clump Weight on 2 MW Floating Offshore Wind Turbine Mooring System in Extreme Sea Condition and Shallow Water*, in *Department of Engineering Science and Ocean Engineering*. 2023, National Taiwan University.

doi:10.6342/NTU202500993

Appendix A Appended Papers

A.1 Paper 1

Paper 1:

Assessment of Intact Stability Criteria and Survivability for Semi-submersible FOWT.

Authors: Kuan-Yi Wu[1], Amir Noorizadegan[1], Donghui Chen[2], Kai-Tung Ma[3]

[1]National Taiwan University, Taipei, Taiwan

[2]Genesis Engineering LLC, Houston, Texas, USA

[3]Energy Research Center, National Taiwan University, Taipei, Taiwan

Accepted by the ASME 2025 44nd International Conference on Ocean, Offshore and Arctic Engineering (OMAE2025)

June 22-27, 2025, Vancouver, British Columbia, Canada

This paper is awaiting publication and is therefore not included.

doi:10.6342/NTU202500993

A.2 Paper 2

Paper 2:

Design and Risk Analysis of FOWT Mooring Systems in Typhoon and Earthquake Environment.

Project Manager: Prof. Kai-tung (KT) Ma

Investigators: Donghui Chen, Kuanu-Yi (Zach) Wu, Jeffrey Lai, Alison Liu, and Emily Huang

Offshore Structures & Mooring Engineering Lab (OSMEL)

National Taiwan University (NTU)

Project Period: June 2024 – May 2025

This paper is an industrial project report sponsored by the offshore wind developer Copenhagen Infrastructure Partners (CIP). Due to commercial confidentiality, certain details are not included.

doi:10.6342/NTU202500993

A.3 Paper 3

Paper 3:

Hull and Stability Specification of TaidaFloat Medium Demo.

Authors: Glib Ivanov, Kuanu-Yi (Zach) Wu

Offshore Structures & Mooring Engineering Lab (OSMEL)

National Taiwan University (NTU)

The specification is open source and available to the public. The latest version can be accessed at: https://taidamooring.wixsite.com/taida

doi:10.6342/NTU202500993

A.4 Paper 4

Paper 4:

Choice of Floater: A Comparative Analysis of FOWT Floater Types.

Authors: Kuanu-Yi (Zach) Wu[1], Amir Noorizadegan[2], Zhiyu Jiang[3], Kai-Tung Ma[1]*

[1] *Department of Engineering Science and Ocean Engineering, National Taiwan University, Taiwan*

[2] *Department of Civil Engineering, National Taiwan University, Taiwan*

[3]*Department of Engineering and Science, University of Agder, Norway*

This paper is awaiting submission and is therefore not included.

doi:10.6342/NTU202500993

Appendix B Python Script for MPM Method

```python
import os
import glob
import collections
import xlsxwriter
import OrcFxAPI
import OrcaFun
import re
import numpy as np
import matplotlib.pyplot as plt
from scipy.stats import weibull_min, gumbel_r


simulation_data_path = r'input the file name to read the data'
excel_file_path = r'input the file name to save the result'

# Set global font sizes for all plots
plt.rcParams.update({
    'font.size': 14,
    'axes.titlesize': 16,
    'axes.labelsize': 14,
    'xtick.labelsize': 12,
    'ytick.labelsize': 12,
    'legend.fontsize': 12,
})

# User options at the beginning of the script
def get_user_options():
    print("Do you want to generate plots? (yes/no)")
    plot_choice = input().strip().lower()
    while plot_choice not in ['yes', 'no']:
        print("Please enter 'yes' or 'no':")
        plot_choice = input().strip().lower()
    do_plot = (plot_choice == 'yes')

    print("Do you want to remove outliers? (yes/no)")
    outlier_choice = input().strip().lower()
    while outlier_choice not in ['yes', 'no']:
        print("Please enter 'yes' or 'no':")
        outlier_choice = input().strip().lower()
    remove_outliers_option = (outlier_choice == 'yes')

    return do_plot, remove_outliers_option

# Get user options
DO_PLOT, REMOVE_OUTLIERS = get_user_options()

tracked_properties = ['mpm_tension_line']

def extract_angle(case_name):
    match = re.search(r'_(wi|wa|cu)(\d+)', case_name)
    return int(match.group(2)) if match else 0

def get_period(model):
    general = model.general
    Stage_process = [1]
    period = OrcFxAPI.SpecifiedPeriod(general.StageStartTime[min(Stage_process)], general.StageEndTime[max(Stage_process)])
    return period

def remove_outliers(data):
    data = np.array(data)
    Q1 = np.percentile(data, 25)
```


doi:10.6342/NTU202500993

```
    Q3 = np.percentile(data, 75)
    IQR = Q3 - Q1
    lower_bound = Q1 - 3 * IQR
    upper_bound = Q3 + 3 * IQR
    filtered_data = data[(data >= lower_bound) & (data <= upper_bound)]
    return filtered_data if len(filtered_data) > 0 else data

def extract_peaks_upcrossing(tension_data):
    tension_array = np.array(tension_data)
    mean_tension = np.mean(tension_array)
    std_tension = np.std(tension_array)
    threshold = mean_tension + 4 * std_tension    # Modified threshold: mean + 4*std
    upcrossings = []
    for i in range(1, len(tension_array)):
        if tension_array[i-1] <= threshold and tension_array[i] > threshold:
            upcrossings.append(i)

    peak_values = []
    peak_indices = []

    # Peaks between up-crossings
    for j in range(len(upcrossings) - 1):
        start_idx = upcrossings[j]
        end_idx = upcrossings[j + 1]
        peak_idx = start_idx + np.argmax(tension_array[start_idx:end_idx])
        peak_value = tension_array[peak_idx]
        if peak_value > threshold:    # Use new threshold
            peak_values.append(peak_value)
            peak_indices.append(peak_idx)

    # First peak before the first up-crossing
    if upcrossings:
        if upcrossings[0] > 0:
            first_segment = tension_array[:upcrossings[0]]
            first_peak_idx = np.argmax(first_segment)
            first_peak_value = first_segment[first_peak_idx]
            if first_peak_value > threshold:    # Use new threshold
                peak_values.append(first_peak_value)
                peak_indices.append(first_peak_idx)

        # Last peak after the last up-crossing
        if upcrossings[-1] < len(tension_array) - 1:
            last_segment = tension_array[upcrossings[-1]:]
            last_peak_idx = upcrossings[-1] + np.argmax(last_segment)
            last_peak_value = tension_array[last_peak_idx]
            if last_peak_value > threshold:    # Use new threshold
                peak_values.append(last_peak_value)
                peak_indices.append(last_peak_idx)

    # If no up-crossings, find the global maximum if it's above the threshold
    if not upcrossings:
        peak_idx = np.argmax(tension_array)
        peak_value = tension_array[peak_idx]
        if peak_value > threshold:
            peak_values.append(peak_value)
            peak_indices.append(peak_idx)

    return peak_values, peak_indices, mean_tension

def fit_weibull_and_gumbel(peak_values, num_simulations=10000):
    peak_values = np.array(peak_values)
    # Remove outliers if the option is enabled
    if REMOVE_OUTLIERS:
        filtered_peaks = remove_outliers(peak_values)
        if len(filtered_peaks) < 2:
            filtered_peaks = peak_values    # Fallback if too few points after filtering
    else:
```


doi:10.6342/NTU202500993

```
            filtered_peaks = peak_values

        n = len(filtered_peaks)
        k, gamma, lambda_ = weibull_min.fit(filtered_peaks)

        simulated_maxima = []
        for _ in range(num_simulations):
            samples = weibull_min.rvs(k, loc=gamma, scale=lambda_, size=n)
            max_value = np.max(samples)
            simulated_maxima.append(max_value)

        mu, beta = gumbel_r.fit(simulated_maxima)

        p = 0.37
        MPM = gumbel_r.ppf(p, mu, beta)

        return MPM, mu, beta, k, gamma, lambda_, n

def plot_weibull_only(peak_values, k, gamma, lambda_, title):
        peak_values = np.array(peak_values)
        plt.figure(figsize=(10, 6))
        counts, bins, _ = plt.hist(peak_values, bins=50, density=True, alpha=0.6, color='b', label='Peak Values Histogram')
        x = np.linspace(min(bins), max(bins), 100)
        fx = weibull_min.pdf(x, k, loc=gamma, scale=lambda_)
        plt.plot(x, fx, 'b-', lw=2, label=r'$f_X(y)$ (Weibull)')

        plt.xlabel('Peak Tension (kN)')
        plt.ylabel('Density')
        plt.title(f'Weibull Fit - {title}')
        plt.legend()
        plt.grid(True)
        plt.show()

def plot_weibull_gumbel(peak_values, mu, beta, k, gamma, lambda_, n, title):
        peak_values = np.array(peak_values)
        plt.figure(figsize=(10, 6))
        counts, bins, _ = plt.hist(peak_values, bins=50, density=True, alpha=0.6, color='b', label='Peak Values Histogram')
        x = np.linspace(min(bins), max(bins), 100)
        fx = weibull_min.pdf(x, k, loc=gamma, scale=lambda_)
        plt.plot(x, fx, 'b-', lw=2, label=r'$f_X(y)$ (Weibull)')
        Fx = weibull_min.cdf(x, k, loc=gamma, scale=lambda_)
        fy = n * (Fx ** (n - 1)) * fx
        plt.plot(x, fy, 'r-', lw=2, label=r'$f_Y(y) = n [F_X(y)]^{n-1} f_X(y)$')
        gumbel_pdf = gumbel_r.pdf(x, mu, beta)
        plt.plot(x, gumbel_pdf, 'r--', lw=1, label=f'Gumbel Fit (μ={mu:.2f}, β={beta:.2f})')

        plt.xlabel('Peak Tension (kN)')
        plt.ylabel('Density')
        plt.title(f'Weibull and Gumbel Fit - {title}')
        plt.legend()
        plt.grid(True)
        plt.show()

def plot_weibull_gumbel_mpm(peak_values, mu, beta, k, gamma, lambda_, n, title, MPM, original_MPM, seed_max):
        peak_values = np.array(peak_values)
        plt.figure(figsize=(10, 6))
        counts, bins, _ = plt.hist(peak_values, bins=50, density=True, alpha=0.6, color='b', label='Peak Values Histogram')
        x = np.linspace(min(bins), max(bins), 100)
        fx = weibull_min.pdf(x, k, loc=gamma, scale=lambda_)
        plt.plot(x, fx, 'b-', lw=2, label=r'$f_X(y)$ (Weibull)')
        Fx = weibull_min.cdf(x, k, loc=gamma, scale=lambda_)
        fy = n * (Fx ** (n - 1)) * fx
        plt.plot(x, fy, 'r-', lw=2, label=r'$f_Y(y) = n [F_X(y)]^{n-1} f_X(y)$')
```


doi:10.6342/NTU202500993

```python
    gumbel_pdf = gumbel_r.pdf(x, mu, beta)
    plt.plot(x, gumbel_pdf, 'r--', lw=1, label=f'Gumbel Fit (μ={mu:.2f}, β={beta:.2f})')

    MPM_y = gumbel_r.pdf(MPM, mu, beta)
    plt.plot(MPM, MPM_y, 'yo', markersize=10, label='MPM (37th Percentile, Capped)')
    plt.annotate('MPM (Capped)', xy=(MPM, MPM_y), xytext=(MPM + 0.5, MPM_y + 0.1),
                 arrowprops=dict(facecolor='black', shrink=0.05))

    if original_MPM > seed_max:
        original_MPM_y = gumbel_r.pdf(original_MPM, mu, beta)
        plt.plot(original_MPM, original_MPM_y, 'go', markersize=10, label='Original MPM (37th Percentile)')
        plt.annotate('Original MPM', xy=(original_MPM, original_MPM_y),
                     xytext=(original_MPM + 0.5, original_MPM_y + 0.05),
                     arrowprops=dict(facecolor='green', shrink=0.05))

    plt.xlabel('Peak Tension (kN)')
    plt.ylabel('Density')
    plt.title(f'Weibull, Gumbel, and MPM - {title}')
    plt.legend()
    plt.grid(True)
    plt.show()

def plot_timeseries(tension_data, peak_indices, mean_tension, threshold, experiment_name, seed_idx):
    tension_array = np.array(tension_data)
    time = np.arange(len(tension_array))
    plt.figure(figsize=(12, 6))
    plt.plot(time, tension_array, 'b-', label='Time Series')
    plt.axhline(mean_tension, color='r', linestyle='--', label=f'Mean = {mean_tension:.2f}')
    plt.axhline(threshold, color='g', linestyle='--', label=f'Threshold = {threshold:.2f}')  # Add threshold line
    plt.plot(time[peak_indices], tension_array[peak_indices], 'go', label='Chosen Peaks')
    plt.xlabel('Time Step')
    plt.ylabel('Tension (kN)')
    plt.title(f'Time Series with Peaks - {experiment_name} (Seed {seed_idx + 1})')
    plt.legend()
    plt.grid(True)
    plt.show()

def get_mpm_tension_line(model):
    _, lines = OrcaFun.determine_lines(model)
    max_tensions = []

    for line in lines:
        tension = line.RangeGraph('Effective Tension')
        max_tensions.append(max(tension.Max))

    max_tension = max(max_tensions)
    max_tension_line = lines[max_tensions.index(max_tension)]

    tension_series = max_tension_line.TimeHistory("Effective tension",
                                                  OrcaFun.get_period(model),
                                                  objectExtra=OrcFxAPI.oeEndA)

    peak_values, peak_indices, mean_tension = extract_peaks_upcrossing(tension_series)

    if len(peak_values) < 2:
        print(f"Warning: Insufficient peaks for {max_tension_line.Name}. Using simplified MPM.")
        tension_array = np.array(tension_series)
        mean_tension = np.mean(tension_array)
        std_tension = np.std(tension_array)
        mpm = mean_tension + (0.57721 * std_tension * np.sqrt(6) / np.pi)
        return {
            'line_name': max_tension_line.Name,
            'lay_azimuth': round(max_tension_line.LayAzimuth, 1),
            'mpm': mpm,
```


doi:10.6342/NTU202500993

```python
            'max': max_tension,
            'mean': mean_tension,
            'tension_series': tension_series,
            'peak_values': peak_values,
            'peak_indices': peak_indices
        }

    MPM, mu, beta, k, gamma, lambda_, n = fit_weibull_and_gumbel(peak_values)

    return {
        'line_name': max_tension_line.Name,
        'lay_azimuth': round(max_tension_line.LayAzimuth, 1),
        'mpm': MPM,
        'max': max_tension,
        'mean': mean_tension,
        'tension_series': tension_series,
        'peak_values': peak_values,
        'peak_indices': peak_indices,
        'mu': mu,
        'beta': beta,
        'k': k,
        'gamma': gamma,
        'lambda': lambda_,
        'n': n
    }

def process_simulation(model, exp_name, seed_num):
    result = get_mpm_tension_line(model)
    seed_max = max(result['peak_values']) if result['peak_values'] else result['max']
    original_mpm = result['mpm']    # Store the original uncapped MPM

    notice = ""
    if result['mpm'] > seed_max:
        notice = f" [Original MPM ({result['mpm']:.2f}) exceeds Seed Max ({seed_max:.2f}), capped at Seed Max]"
    result['original_mpm'] = original_mpm    # Keep the original value
    result['mpm'] = min(result['mpm'], seed_max)    # Cap the reported MPM

    print(f"{exp_name}, Seed {seed_num}: Number of peaks = {len(result['peak_values'])}{notice}")

    if DO_PLOT:
        # Calculate threshold (same as in extract_peaks_upcrossing)
        tension_array = np.array(result['tension_series'])
        mean_tension = result['mean']
        std_tension = np.std(tension_array)
        threshold = mean_tension + 4 * std_tension
        # Pass threshold to plot_timeseries
        plot_timeseries(result['tension_series'], result['peak_indices'], mean_tension, threshold, exp_name, seed_num - 1)
        if 'mu' in result:
            plot_weibull_only(result['peak_values'], result['k'], result['gamma'], result['lambda'],
                              f"{exp_name} (Seed {seed_num})")
            plot_weibull_gumbel(result['peak_values'], result['mu'], result['beta'], result['k'],
                                result['gamma'], result['lambda'], result['n'],
                                f"{exp_name} (Seed {seed_num})")
            plot_weibull_gumbel_mpm(result['peak_values'], result['mu'], result['beta'], result['k'],
                                    result['gamma'], result['lambda'], result['n'],
                                    f"{exp_name} (Seed {seed_num})", result['mpm'], result['original_mpm'], seed_max)

    return result

def save_results_to_excel(data, excel_file_path):
    workbook = xlsxwriter.Workbook(excel_file_path)
    worksheet = workbook.add_worksheet()
    worksheet.write(0, 0, "Experiment")
    worksheet.write(0, 1, "Average MPM (kN)")    # Capped MPM
```


doi:10.6342/NTU202500993

```
    worksheet.write(0, 2, "Average Original MPM (kN)")    # Uncapped MPM
    worksheet.write(0, 3, "Average Max (kN)")
    worksheet.write(0, 4, "Critical Line")
    worksheet.write(0, 5, "Lay Azimuth (°)")
    worksheet.write(0, 6, "Number of Seeds")

    row = 1
    for exp_name, properties in data.items():
        worksheet.write(row, 0, exp_name)
        if 'mpm_tension_line' in properties:
            mpm_values = [result['mpm'] for result in properties['mpm_tension_line']]    # Capped
            original_mpm_values = [result['original_mpm'] for result in properties['mpm_tension_line']]    # Uncapped
            max_values = [result['max'] for result in properties['mpm_tension_line']]
            line_names = [result['line_name'] for result in properties['mpm_tension_line']]
            lay_azimuths = [result['lay_azimuth'] for result in properties['mpm_tension_line']]

            worksheet.write(row, 1, np.mean(mpm_values))
            worksheet.write(row, 2, np.mean(original_mpm_values))    # New column for original MPM
            worksheet.write(row, 3, np.mean(max_values))
            worksheet.write(row, 4, max(set(line_names), key=line_names.count))
            worksheet.write(row, 5, lay_azimuths[line_names.index(max(set(line_names), key=line_names.count))])
            worksheet.write(row, 6, len(mpm_values))
            row += 1

    workbook.close()
    print(f"All results saved to Excel file: {os.path.abspath(excel_file_path)}")

def split_experiment_name(exp_name):
    last_underscore_index = exp_name.rfind('_')
    if last_underscore_index != -1:
        name_part = exp_name[:last_underscore_index]
        group_part = exp_name[last_underscore_index + 1:]
    else:
        name_part = exp_name
        group_part = ''
    return name_part, group_part

def main():
    sim_name_pattern = '*.sim'

    sim_paths = glob.glob(os.path.join(simulation_data_path, sim_name_pattern))
    print(f'Found {len(sim_paths)} simulation paths')

    experiments = set()
    for path in sim_paths:
        sim_name = os.path.basename(path)
        name_part, _ = split_experiment_name(sim_name)
        experiments.add(name_part)

    sorted_experiments = sorted(experiments, key=extract_angle)
    all_results = {}

    for exp_name in sorted_experiments:
        simulations = []
        exp_paths = [path for path in sim_paths if os.path.basename(path).startswith(exp_name)]
        print(f'\nFound {len(exp_paths)} simulations for {exp_name}')

        for path in exp_paths:
            try:
                print(f'Loading simulation {path}')
                model = OrcFxAPI.Model()
                model.LoadSimulation(path)
                print('Finished loading simulation')
```


doi:10.6342/NTU202500993

```
                simulations.append(model)
            except OrcFxAPI.DLLError as e:
                print(f'Error loading simulation {path}: {e}')
                continue

        simulation_results = collections.defaultdict(list)

        for seed_num, model in enumerate(simulations, 1):
            try:
                result = process_simulation(model, exp_name, seed_num)
                simulation_results['mpm_tension_line'].append(result)
            except Exception as e:
                print(f'Error processing {exp_name}, Seed {seed_num}: {e}')
                continue

        all_results[exp_name] = simulation_results

    save_results_to_excel(all_results, excel_file_path)

if __name__ == "__main__":
    main()
```


doi:10.6342/NTU202500993